

Metasurfaces-Integrated Doubly-Dispersive MIMO: Channel Modeling and Optimization

Kuranage Roche Rayan Ranasinghe^[0000-0002-6834-8877],
Hyeon Seok Rou^[0000-0003-3483-7629],
Iván Alexander Morales Sandoval^[0000-0002-8601-5451],
Giuseppe Thadeu Freitas de Abreu^[0000-0002-5018-8174] and
George C. Alexandropoulos^[0000-0002-6587-1371]

Abstract The doubly-dispersive (DD) channel structure has played a pivotal role in wireless communications, particularly in high-mobility scenarios and integrated sensing and communications (ISAC), due to its ability to capture the key fading effects experienced by a transmitted signal as it propagates through a dynamic medium. However, extending the DD framework to multiple-input multiple-output (MIMO) systems, especially in environments artificially enhanced by reconfigurable intelligent surfaces (RISs) and stacked intelligent metasurfaces (SIM), remains a challenging open problem. In this chapter, a novel metasurfaces-parametrized DD (MPDD) channel model that integrates an arbitrary number of RISs, while also incorporating SIM at both the transmitter and receiver is introduced. Next, the application of this model to some key waveforms optimized for DD environments – namely orthogonal frequency division multiplexing (OFDM), orthogonal time frequency space (OTFS), and affine frequency division multiplexing (AFDM) – is discussed. Finally, the programmability of the proposed model is highlighted through an illustrative application, demonstrating its potential for enhancing waveform performance in SIM-assisted wireless systems.

Kuranage Roche Rayan Ranasinghe
Constructor University (previously known as Jacobs University Bremen), Campus Ring 1, 28759 Bremen, Germany, e-mail: kranasinghe@constructor.university

Hyeon Seok Rou
Constructor University (previously known as Jacobs University Bremen), Campus Ring 1, 28759 Bremen, Germany, e-mail: hrou@constructor.university

Iván Alexander Morales Sandoval
Constructor University (previously known as Jacobs University Bremen), Campus Ring 1, 28759 Bremen, Germany, e-mail: imorales@constructor.university

Giuseppe Thadeu Freitas de Abreu
Constructor University (previously known as Jacobs University Bremen), Campus Ring 1, 28759 Bremen, Germany, e-mail: gabreu@constructor.university

George C. Alexandropoulos
National and Kapodistrian University of Athens, 16122 Athens, Greece, e-mail: alexandg@di.uoa.gr

1 Introduction

Next generation wireless communication systems are anticipated to enable a diverse range of new applications, including vehicle-to-everything (V2X) and aerial communications [1], internet of things (IoT) networks [2], and non-terrestrial networks (NTNs) such as low-earth orbit (LEO) satellite networks [3]. Due to the intrinsic nature of the resulting high-mobility environment in these systems [4], there is a great demand for accurate channel models and robust detectors/estimators to encapsulate such surroundings.

However, high-mobility communication scenarios pose significant challenges due to the time-frequency selectivity in time-varying multipath conditions [5]. This necessitates the use of doubly-dispersive (DD) channel models [6, 7, 83, 8], which have recently been leveraged for devising various advanced communication techniques [9, 10, 11, 12, 13, 14]. A key development in this area is the application of DD channel models for radar parameter estimation (RPE), leading to communication-centric (CC) integrated sensing and communications (ISAC) [48, 19, 20, 21, 22, 46, 47, 23, 24, 25, 43, 45, 67] which enables both sensing and communications functionalities. CC-ISAC offers a compelling ISAC solution in high-mobility scenarios by integrating RPE techniques with traditional signal processing methods, such as de-chirping in affine frequency division multiplexing (AFDM) [26], bilinear inference [27, 28, 29], and blind covariance-based detection [30, 31]. This allows ISAC to be implemented in mono-, bi-, and multi-static configurations [32].

The effective waveform design constitutes a crucial aspect for the use of DD channels. While many such waveforms exist in literature, three of the primary candidates include:

- **Orthogonal frequency division multiplexing (OFDM)**: A widely adopted waveform with useful RPE properties [36], but susceptible to severe inter-carrier interference in high-mobility scenarios [37].
- **Orthogonal time frequency space (OTFS)**: A two-dimensional (2D) modulation scheme embedding data in the delay-Doppler domain, offering robustness to DD effects, but requiring higher implementation complexity [9] relative to OFDM.
- **Affine frequency division multiplexing (AFDM)**: A recently proposed alternative [33, 34, 35] achieving optimal diversity in DD channels with a similar implementation complexity to OFDM, though facing practical challenges in chirp signal generation [38].

Recent studies have shown that these waveforms share structural similarities within the DD model, enabling unified system design approaches [8]. However, existing unifying work is limited to single-input single-output (SISO) systems, despite the established role of multiple-input multiple-output (MIMO) in modern wireless networks, including emerging paradigms such as extremely large MIMO [41, 42] and reconfigurable metasurfaces [44, 49].

Motivated by these advancements, in this chapter, a novel metasurfaces-parametrized DD (MPDD) MIMO channel model incorporating multi-functional metasurfaces,

such as reconfigurable intelligent surfaces (RISs) [50, 71, 44, 49], dynamic metasurfaces antennas [81, 82], and stacked intelligent metasurfaces (SIM) [51, 52, 53] is proposed, which is amenable to optimization for enhancing high-mobility wireless communications. The key contributions of this chapter are the following:

- Development of a MPDD MIMO channel model integrating transmitter (TX) and receiver (RX) SIM alongside multiple RISs, suitable for high-mobility and CC-ISAC applications.
- Derivation of end-to-end time-domain (TD) received signal expressions and effective channel matrices for OFDM, OTFS, and AFDM, facilitating ISAC objectives.
- Optimization of SIM for enhanced signal reception, employing a Gaussian Belief Propagation (GaBP)-based detector, demonstrating significant performance gains over conventional DD models.

Notation: All scalars are represented by upper or lowercase letters, while column vectors and matrices are denoted by bold lowercase and uppercase letters, respectively. The diagonal matrix constructed from vector \mathbf{a} is denoted by $\text{diag}(\mathbf{a})$, while \mathbf{A}^\top , \mathbf{A}^H , $\mathbf{A}^{1/2}$, and $[\mathbf{A}]_{i,j}$ denote the transpose, Hermitian, square root, and the (i, j) -th element of a matrix \mathbf{A} , respectively. The convolution and Kronecker product are respectively denoted by $*$ and \otimes , while \mathbf{I}_N and \mathbf{F}_N represent the $N \times N$ identity and the normalized N -point discrete Fourier transform (DFT) matrices, respectively. The sinc function is expressed as $\text{sinc}(a) \triangleq \frac{\sin(\pi a)}{\pi a}$, whereas $j \triangleq \sqrt{-1}$ denotes the elementary complex number.

2 Preliminaries

In this section, some preliminary background on the SISO and MIMO DD channel model as well as the RIS and SIM technologies is provided.

2.1 SISO Doubly-Dispersive Channel Model

Consider a wireless channel between a single-antenna transmitter and single-antenna receiver, modeled using P significant propagation paths. Each p -th resolvable path, with $p \in 1, \dots, P$, is characterized by a complex fading coefficient $h_p \in \mathbb{C}$, a path delay $\tau_p \in [0, \tau^{\max}]$, and a Doppler shift $\nu_p \in [-\nu^{\max}, +\nu^{\max}]$. The delay and Doppler spreads of this DD channel are determined by the maximum delay τ^{\max} in seconds and the maximum Doppler shift $\pm\nu^{\max}$ in Hz.

The channel behavior is described by the linear time-variant (LTV)¹ relationship between the input and output signals, and is most commonly represented as a time-

¹ The term “linear time-variant (LTV) system” is distinct from linear systems with time-varying delays (i.e., $\tau_p(t)$), commonly also referred to as LTV. Herein, only time-invariant delays are considered, in line with prior studies [54, 55, 34].

variant impulse response function (TVIRF) in the time-delay domain given by [8]

$$h^{\text{TD}}(t, \tau) \triangleq \sum_{p=1}^P h_p e^{j2\pi\nu_p t} \delta(\tau - \tau_p), \quad (1)$$

where t and τ denote instantaneous time and delay, respectively, and $\delta(x)$ is the unit impulse function. Alternative representations also exist in other domains via appropriate linear transforms [56]. For example, the time-frequency representation, known as time-variant transfer function (TVTF), is obtained through a Fourier transform (FT) over the delay domain, $\mathcal{F}[\cdot]$, and is represented as follows:

$$h^{\text{TF}}(t, f) \triangleq \mathcal{F} [h^{\text{TD}}(t, \tau)] = \sum_{p=1}^P h_p e^{j2\pi\nu_p t} e^{-j2\pi\tau_p f}. \quad (2)$$

Similarly, the delay-Doppler representation, termed Doppler-variant impulse response function (DVIRF), is obtained via an FT over the time domain as

$$h^{\text{DD}}(\nu, \tau) \triangleq \sum_{p=1}^P h_p \delta(\nu - \nu_p) \delta(\tau - \tau_p). \quad (3)$$

Remark 1 (DD Channel Assumptions) The channel models presented in expressions (1)–(3) are based on a practical approximation of the true DD wireless channel (resulting from the incompatibility of the bandwidth-limited assumption and the temporally-limited assumption of the signals), represented in terms of a finite number of significant delay and Doppler frequency taps, which is known to generally work well [57, 54], especially under the underspread environment assumption, i.e., the maximum delay spread $\tau_{\max} - \tau_{\min}$ is smaller than T , the maximum Doppler spread $\nu_{\max} - \nu_{\min}$ is smaller than $\frac{1}{T}$, and $\tau_{\max} \nu_{\max} \ll 1$, where T is the finite signal period measured in seconds.

Hereafter, without loss of generality (wlg), the time-delay representation in expression (1) is chosen to simplify the upcoming derivations for arbitrary TD signals. For receiver designs based on the SISO DD channel model leveraged for ISAC, the reader is referred to [25].

2.2 MIMO Doubly-Dispersive Channel Model

Let $\phi \in [0, \pi]$ denote the arbitrary angle-of-arrival (AoA) or angle-of-departure (AoD) of a channel propagation path to (or from) a uniform linear array (ULA) with A antenna elements. Then, the array response vector $\mathbf{a}(\phi) \in \mathbb{C}^{A \times 1}$ is defined as

$$\mathbf{a}(\phi) \triangleq \frac{1}{\sqrt{A}} \left[1, e^{-j\frac{2\pi}{\lambda} d \sin(\phi)}, \dots, e^{-j\frac{2\pi}{\lambda} (A-1) d \sin(\phi)} \right]^{\text{T}}, \quad (4)$$

where λ indicates the wavelength and d is the antenna spacing, which is usually set as $d = \lambda/2$ [58].

Similarly, for a uniform planar array (UPA) with $B \triangleq B_x B_z$ elements², the response vector corresponding to a path impinging onto (or outgoing from) the array at the elevation and azimuth angles $\theta \in [0, \pi]$ and $\phi \in [-\frac{\pi}{2}, \frac{\pi}{2}]$ is given by [61]

$$\mathbf{b}(\phi, \theta) \triangleq \frac{1}{\sqrt{B_x B_z}} \mathbf{b}_x(\phi, \theta) \otimes \mathbf{b}_z(\theta) \in \mathbb{C}^{B \times 1}, \quad (5)$$

where the x - and z -axis steering vectors $\mathbf{b}_x(\phi, \theta) \in \mathbb{C}^{B_x \times 1}$ and $\mathbf{b}_z(\theta) \in \mathbb{C}^{B_z \times 1}$ are respectively defined as

$$\mathbf{b}_x(\phi, \theta) \triangleq \left[1, e^{-j \frac{2\pi d_x}{\lambda} \sin(\phi) \sin(\theta)}, \dots, e^{-j \frac{2\pi d_x}{\lambda} (B_x - 1) \sin(\phi) \sin(\theta)} \right]^\top, \quad (6a)$$

and

$$\mathbf{b}_z(\theta) \triangleq \left[1, e^{-j \frac{2\pi d_z}{\lambda} \cos(\theta)}, \dots, e^{-j \frac{2\pi d_z}{\lambda} (B_z - 1) \cos(\theta)} \right]^\top, \quad (6b)$$

with d_x and d_z being the element spacing in the UPA's x - and z -axis directions, respectively, which are usually set as $d_x = d_z = \lambda/2$.

Subsequently, the MIMO equivalent of expression (1) defined in Section 2.1, for the case with N_T transmit antennas and N_R receive antennas, $\mathbf{H}^{\text{TD}}(t, \tau) \in \mathbb{C}^{N_R \times N_T}$, is given by

$$\mathbf{H}^{\text{TD}}(t, \tau) \triangleq \sqrt{\frac{N_T N_R}{P}} \sum_{p=1}^P h_p \cdot e^{j2\pi\nu_p t} \delta(\tau - \tau_p) \mathbf{a}_R(\phi_p^{\text{in}}) \mathbf{a}_T^H(\phi_p^{\text{out}}), \quad (7)$$

where $\mathbf{a}_R(\phi_p^{\text{in}})$ and $\mathbf{a}_T(\phi_p^{\text{out}})$ are the receive and transmit array response vectors, respectively, corresponding to the p -th path with AoA ϕ_p^{in} and AoD ϕ_p^{out} , respectively.

2.3 RIS Response Model

Consider a wireless scenario involving K RISs, where each RIS comprises $J \triangleq J_x J_z$ reflective meta-atoms with tunable responses. Here, J_x and J_z represent the number of meta-atoms along the x - and z -axes, respectively. The reflective phase response of each j -th meta-atom ($j \in \{1, \dots, J\}$) within the k -th RIS ($k \in \{1, \dots, K\}$) is denoted by $\phi_j^k \in [0, 2\pi)$. Consequently, the phase configuration of the k -th RIS can be represented by the $J \times J$ phase matrix Φ_k , which is given by [80]:

$$\Phi_k \triangleq \text{diag} \left(\left[e^{j\phi_1^k}, \dots, e^{j\phi_J^k} \right] \right). \quad (8)$$

² Without loss of generality, the UPA is aligned parallel to the y direction with elements occupying space in the x and z dimensions. The generalization to arbitrary axes is trivial; some other orientations are discussed in [60, 42].

2.4 SIM Response Model

Consider a SIM consisting of Q layers of transmissive metasurfaces arranged in parallel with minimal separation. Each metasurface is composed of $M \triangleq M_x M_z$ response-tunable meta-atoms, where M_x and M_z denote the number of meta-atoms along the x - and z -axis per layer, respectively. Next, the following $M \times M$ matrix is defined, which encapsulates the effective tunable phase shifts of all M meta-atoms embedded in each q -th ($q \in \mathcal{Q} \triangleq \{1, \dots, Q\}$) metasurface layer of the SIM, as follows:

$$\mathbf{\Psi}_q \triangleq \text{diag} \left(\left[e^{J\zeta_1^q}, \dots, e^{J\zeta_M^q} \right] \right), \quad (9)$$

where $\zeta_m^q \in [0, 2\pi) \forall q \in \mathcal{Q}$ and $\forall m \in \mathcal{M} \triangleq \{1, \dots, M\}$ represents the transmissive phase response of the m -th meta-atom lying on the q -th metasurface layer.

The transmission matrix between each $(q-1)$ -th and q -th layer of the SIM, for all $q \in \mathcal{Q} \setminus 1$, is denoted as $\mathbf{\Gamma}_q \in \mathbb{C}^{M \times M}$. According to Rayleigh-Sommerfeld diffraction theory, each (m, m') -th element (where $m, m' \in \mathcal{M}$) of $\mathbf{\Gamma}_q$ represents the diffraction coefficient between the m' -th meta-atom on the $(q-1)$ -th metasurface and the m -th meta-atom on the q -th metasurface, and is given by [61]:

$$\gamma_{m,m'}^q \triangleq \frac{\rho_t \cos(\epsilon_{m,m'}^q)}{d_{m,m'}^q} \left(\frac{1}{2\pi d_{m,m'}^q} - \frac{J}{\lambda} \right) e^{J2\pi \frac{d_{m,m'}^q}{\lambda}}, \quad (10)$$

where ρ_t is the square measure occupied by each meta-atom in the SIM, $\epsilon_{m,m'}^q$ denotes the angle between the propagation and normal direction of the $(q-1)$ -th metasurface layer, and $d_{m,m'}^q$ represents the propagation distance.

Placing the SIM very close to an N_T -element TX ULA with adjacent inter-element spacing $\lambda/2$, let us define $\mathbf{\Gamma}_1 \triangleq [\gamma_1^1, \dots, \gamma_{N_T}^1] \in \mathbb{C}^{M \times N_T}$ with $\gamma_{n_T}^1 \in \mathbb{C}^{M \times 1}$ (with $n_T = 1, \dots, N_T$) representing the transmission vector from the n_T -th transmit antenna to the innermost metasurface layer of the SIM, whose m -th element γ_{m,n_T}^1 is obtained by substituting $\epsilon_{m,m'}^q$ and $d_{m,m'}^q$ in expression (10) with ϵ_{m,n_T}^1 and d_{m,n_T}^1 , respectively.

Bridging the concepts introduced above and defining $\mathcal{Z} \triangleq \{\mathbf{\Psi}_1, \dots, \mathbf{\Psi}_Q\}$, the overall $M \times N_T$ propagation matrix from the TX antenna elements to the meta-atoms of the Q -th SIM layer can be expressed as follows:

$$\Upsilon_T(\mathcal{Z}) \triangleq \prod_{q=1}^Q \mathbf{\Psi}_{Q-q+1} \mathbf{\Gamma}_{Q-q+1}. \quad (11)$$

Similarly, a SIM of \tilde{Q} layers of transmissive metasurfaces, each comprising $\tilde{M} \triangleq \tilde{M}_x \tilde{M}_z$ response-tunable meta-atoms with \tilde{M}_x and \tilde{M}_z being the number of meta-atoms in the x - and z -axis on each layer, respectively, placed very close to an N_R -element RX ULA with adjacent inter-element spacing $\lambda/2$, results in the following overall $N_R \times \tilde{M}$ propagation matrix from the SIM to the RX antenna array:

$$\Upsilon_{\mathbf{R}}(\tilde{\mathcal{Z}}) \triangleq \prod_{\tilde{q}=1}^{\tilde{Q}} \Xi_{\tilde{q}} \Delta_{\tilde{q}}, \quad (12)$$

where $\Xi_{\tilde{q}} \in \mathbb{C}^{\tilde{M} \times \tilde{M}} \forall \tilde{q} \in \{2, \dots, \tilde{Q}\}$ is the transmission matrix between the \tilde{q} -th and $(\tilde{q} - 1)$ -th layer of the SIM, whose elements are defined similar to (10) as

$$\xi_{\tilde{m}, \tilde{m}'}^{\tilde{q}} \triangleq \frac{\rho_r \cos(\tilde{\epsilon}_{\tilde{m}, \tilde{m}'}^{\tilde{q}})}{\tilde{d}_{\tilde{m}, \tilde{m}'}^{\tilde{q}}} \left(\frac{1}{2\pi \tilde{d}_{\tilde{m}, \tilde{m}'}^{\tilde{q}}} - \frac{J}{\lambda} \right) e^{J2\pi \frac{\tilde{q}}{\lambda} \tilde{m}, \tilde{m}'}. \quad (13)$$

In this expression, ρ_r denotes the square measure occupied by each meta-atom in the RX-SIM, $\tilde{\epsilon}_{\tilde{m}, \tilde{m}'}^{\tilde{q}}$ is the angle between the propagation and normal direction of the $(\tilde{q} - 1)$ -th metasurface layer, and $\tilde{d}_{\tilde{m}, \tilde{m}'}^{\tilde{q}}$ corresponds to the propagation distance. Subsequently, $\Xi_1 \triangleq [\xi_1^1, \dots, \xi_{N_{\mathbf{R}}}^1]^T \in \mathbb{C}^{N_{\mathbf{R}} \times \tilde{M}}$ with $\xi_{n_{\mathbf{R}}}^1 \in \mathbb{C}^{\tilde{M} \times 1}$ ($n_{\mathbf{R}} = 1, \dots, N_{\mathbf{R}}$) denoting the transmission vector from the $n_{\mathbf{R}}$ -th receive antenna to the innermost SIM layer, whose \tilde{m} -th element $\xi_{\tilde{m}, n_{\mathbf{R}}}^1$ with $m \in \tilde{\mathcal{M}} \triangleq \{1, \dots, \tilde{M}\}$ is defined similarly to $\gamma_{m, n_{\mathbf{T}}}^1$, but using expression (13). Finally, $\Delta_{\tilde{q}} \forall \tilde{q} \in \tilde{\mathcal{Q}} \triangleq \{1, \dots, \tilde{Q}\}$ defined similar to expression (9) including the effective tunable phase responses $\tilde{\zeta}_{\tilde{m}}^{\tilde{q}} \in [0, 2\pi) \forall \tilde{q} \in \tilde{\mathcal{Q}}$ and $\forall \tilde{m} \in \tilde{\mathcal{M}}$ with $\tilde{\mathcal{Z}} \triangleq \{\Delta_1, \dots, \Delta_{\tilde{Q}}\}$ is given by

$$\Delta_{\tilde{q}} \triangleq \text{diag} \left(\left[e^{J\tilde{\zeta}_1^{\tilde{q}}}, \dots, e^{J\tilde{\zeta}_{\tilde{M}}^{\tilde{q}}} \right] \right). \quad (14)$$

3 The Proposed MPDD MIMO Channel Model

Consider the MIMO system illustrated in Fig. 1, where a transmitter with an $N_{\mathbf{T}}$ -element ULA and a Q -layered SIM, and a receiver equipped with a \tilde{Q} -layered SIM and a ULA-based front-end with $N_{\mathbf{R}}$ antennas, establish a communications link. Both the TX and RX SIM are placed very close to their respective antenna arrays, as described in Section 2.4, and are respectively denoted as TX-SIM and RX-SIM. In addition, as clarified in the figure, the MIMO system operates within a smart wireless environment [71] comprising K RISs each consisting of J response-tunable reflective meta-atoms, as described in Section 2.3.

The complex-valued $N_{\mathbf{R}} \times N_{\mathbf{T}}$ end-to-end MPDD smart wireless MIMO channel, which is parametrized via the configurations of the TX and RX SIM (i.e., \mathcal{Z} and $\tilde{\mathcal{Z}}$, respectively) as well as the RISs (i.e., $\mathcal{F} \triangleq \{\Phi_1, \dots, \Phi_K\}$), can be expressed as follows³:

$$\mathbf{H}(\mathcal{Z}, \tilde{\mathcal{Z}}, \mathcal{F}, t, \tau) \triangleq \Upsilon_{\mathbf{R}}(\tilde{\mathcal{Z}}) \mathbf{R}_{\text{RX}}^{1/2} \tilde{\mathbf{H}}(\mathcal{F}, t, \tau) \mathbf{R}_{\text{TX}}^{1/2} \Upsilon_{\mathbf{T}}(\mathcal{Z}), \quad (15)$$

³ The proposed MPDD MIMO channel model holds also for cases where any of the SIM or RISs has a non-local structure [62, 63, 79].

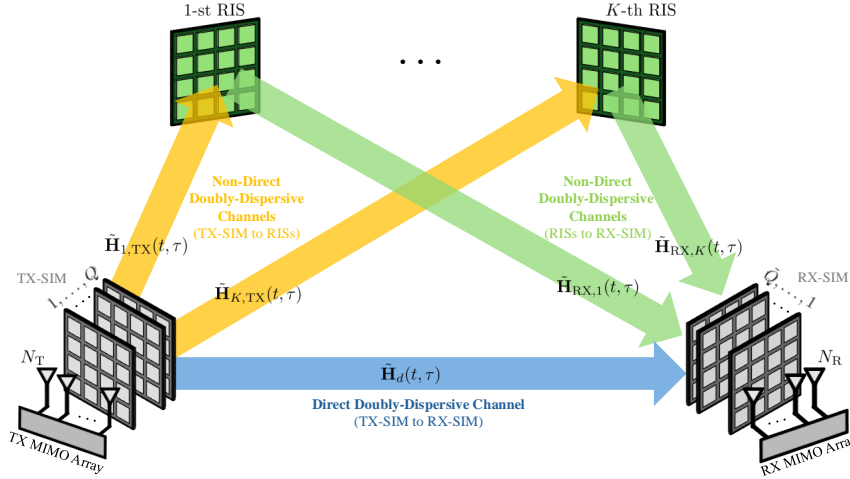


Fig. 1: The considered MPDD MIMO system for high-mobility scenarios, which includes two SIM, one placed very close to the TX and the other very close to the RX, and K RISs within the wireless propagation environment of interest.

where $\mathbf{R}_{\text{TX}} \in \mathbb{C}^{M \times M}$ and $\mathbf{R}_{\text{RX}} \in \mathbb{C}^{\tilde{M} \times \tilde{M}}$ are, respectively, the spatial correlation matrices at the outermost – *i.e.*, respectively the Q -th and \tilde{Q} -th – layer of the TX-SIM and RX-SIM, due to the sub-wavelength spacing of adjacent meta-atoms [68, 69, 70].

Following [61], each (m, m') -th and (\tilde{m}, \tilde{m}') -th elements of \mathbf{R}_{TX} and \mathbf{R}_{RX} in expression (15) are respectively defined as $[\mathbf{R}_{\text{TX}}]_{m, m'} \triangleq \text{sinc}(2d_{m, m'} / \lambda)$ and $[\mathbf{R}_{\text{RX}}]_{\tilde{m}, \tilde{m}'} \triangleq \text{sinc}(2\tilde{d}_{\tilde{m}, \tilde{m}'} / \lambda)$, while the complex-valued $\tilde{M} \times M$ DD RISs-parametrized channel matrix $\tilde{\mathbf{H}}(\mathcal{F}, t, \tau)$ is given by

$$\tilde{\mathbf{H}}(\mathcal{F}, t, \tau) \triangleq \tilde{\mathbf{H}}_d(t, \tau) + \sum_{k=1}^K \tilde{\mathbf{H}}_{\text{RX}, k}(t, \tau) \Phi_k \tilde{\mathbf{H}}_{k, \text{TX}}(t, \tau), \quad (16)$$

where $\tilde{\mathbf{H}}_d(t, \tau) \in \mathbb{C}^{\tilde{M} \times M}$ represents the direct P -path DD MIMO channel between the \tilde{M} -element \tilde{Q} -th layer of the RX-SIM and the M -element Q -th layer of the TX-SIM, which is defined as follows:

$$\tilde{\mathbf{H}}_d(t, \tau) \triangleq \sqrt{\frac{M\tilde{M}}{P}} \sum_{p=1}^P h_p e^{j2\pi\nu_p t} \delta(\tau - \tau_p) \mathbf{b}_R(\phi_p^{\text{in}}, \theta_p^{\text{in}}) \mathbf{b}_T^H(\phi_p^{\text{out}}, \theta_p^{\text{out}}), \quad (17)$$

where $\mathbf{b}_T(\cdot, \cdot) \in \mathbb{C}^{M \times 1}$ and $\mathbf{b}_R(\cdot, \cdot) \in \mathbb{C}^{\tilde{M} \times 1}$ are respectively the UPA response vectors for the TX-SIM and RX-SIM defined in expression (5) in Section 2.2, with $(\phi_p^{\text{in}}, \theta_p^{\text{in}})$ and $(\phi_p^{\text{out}}, \theta_p^{\text{out}})$ being the pairs of azimuth and elevation AoAs and AoDs, respectively, for each p -th signal propagation path. The UPA response matrix associated with a given p -th path is defined as:

$$\mathbf{B}_p \triangleq \mathbf{b}_R \left(\phi_p^{\text{in}}, \theta_p^{\text{in}} \right) \mathbf{b}_T^H \left(\phi_p^{\text{out}}, \theta_p^{\text{out}} \right). \quad (18)$$

Finally, for the sake of clarity, the matrices $\tilde{\mathbf{H}}_{k,\text{TX}}(t, \tau) \in \mathbb{C}^{J \times M}$ and $\tilde{\mathbf{H}}_{\text{RX},k}(t, \tau) \in \mathbb{C}^{\tilde{M} \times J}$ in expression (16) can be expressed similarly to (17) as \tilde{P} - and \tilde{P} -path DD MIMO channels, respectively, namely:

$$\tilde{\mathbf{H}}_{k,\text{TX}}(t, \tau) \triangleq \sqrt{\frac{JM}{\tilde{P}}} \sum_{\tilde{p}=1}^{\tilde{P}} h_{\tilde{p},k} e^{J2\pi\nu_{\tilde{p},k}t} \delta(\tau - \tau_{\tilde{p},k}) \mathbf{B}_{\tilde{p},k}, \quad (19)$$

and

$$\tilde{\mathbf{H}}_{\text{RX},k}(t, \tau) \triangleq \sqrt{\frac{JM}{\tilde{P}}} \sum_{\tilde{p}=1}^{\tilde{P}} h_{\tilde{p},k} e^{J2\pi\nu_{\tilde{p},k}t} \delta(\tau - \tau_{\tilde{p},k}) \mathbf{B}_{\tilde{p},k}. \quad (20)$$

The notation $h_{\tilde{p},k}$ as well as $(\phi_{\tilde{p},k}^{\text{in}}, \theta_{\tilde{p},k}^{\text{in}})$ and $(\phi_{\tilde{p},k}^{\text{out}}, \theta_{\tilde{p},k}^{\text{out}})$ for the complex channel gain and pairs of azimuth and elevation AoAs and AoDs, respectively, for each \tilde{p} -th signal propagation path between the TX-SIM and each k -th RIS, with $\tilde{p} = \{1, \dots, \tilde{P}\}$ will be used henceforth. Similarly, $h_{\tilde{p},k}$ as well as $(\phi_{\tilde{p},k}^{\text{in}}, \theta_{\tilde{p},k}^{\text{in}})$ and $(\phi_{\tilde{p},k}^{\text{out}}, \theta_{\tilde{p},k}^{\text{out}})$ indicate the complex channel gain and pairs of azimuth and elevation AoAs and AoDs, respectively, for each \tilde{p} -th path between each k -th RIS and the RX-SIM, with $\tilde{p} = \{1, \dots, \tilde{P}\}$. The delays and Doppler shifts of the latter paths are denoted by $\tau_{\tilde{p},k}$, $\nu_{\tilde{p},k}$, and $\tau_{\tilde{p},k}$, $\nu_{\tilde{p},k}$, respectively, having similar bounds to τ_p and ν_p defined in Section 2.1.

Remark 2 (Special Cases) Removing the second term with the K summations in expression (16) simplifies the full model to the MIMO channel case including a TX and RX SIM with no RISs present. In addition, removing any of the factors $\Upsilon_R(\tilde{\mathcal{Z}}) \mathbf{R}_{\text{RX}}^{1/2}$ or $\mathbf{R}_{\text{TX}}^{1/2} \Upsilon_T(\mathcal{Z})$ in expression (15), implies a MIMO system lacking a RX-SIM or a TX-SIM, respectively. In the second of the latter two cases, $\tilde{\mathbf{H}}(\mathcal{F}, t, \tau)$ appearing in expressions (15) and (16) models signal propagation directly from the elements of the TX ULA (see the ULA response vector in (4)) to the RX-SIM, via the K RISs. In this case, the size of $\tilde{\mathbf{H}}(\mathcal{F}, t, \tau)$ becomes $\tilde{M} \times N_T$. Alternatively, when only the RX-SIM is missing, $\tilde{\mathbf{H}}(\mathcal{F}, t, \tau)$ will be of size $N_R \times M$. Finally, when none of the SIM are considered, $\mathbf{H}(\mathcal{Z}, \tilde{\mathcal{Z}}, \mathcal{F}, t, \tau) \equiv \tilde{\mathbf{H}}(\mathcal{F}, t, \tau)$ representing the RISs-empowered $N_R \times N_T$ DD MIMO channel. In the absence of RISs and for a single-antenna TX and RX (i.e., $N_T = N_R = 1$), the latter channel model reduces to the model described in [8] and summarized in Section 2.1.

4 Signal Modeling with OFDM, OTFS, and AFDM

In this section, the applicability of the proposed MPDD MIMO channel model is demonstrated by deriving various expressions for the TD received signal corresponding to waveforms such as OFDM, OTFS, and AFDM.

4.1 Arbitrarily Modulated Signals

Consider the deployment of fully digital beamformers in the MIMO system shown in Fig. 1 at its N_T -element TX and N_R -element RX. Let $\mathbf{V} \in \mathbb{C}^{N_T \times d_s}$ and $\mathbf{U} \in \mathbb{C}^{N_R \times d_s}$ represent the transmit and receive digital beamformers, respectively, where $d_s \triangleq \min(N_T, N_R)$ corresponds to the number of independent data streams to be communicated per coherent channel block. In addition, let $\mathbf{s}(t)$ represent the complex-valued and d_s -element transmit signal of any modulation (e.g., OFDM, OTFS, and AFDM) in the TD. Consequently, the d_s -element baseband received signal at a time instant t (after the digital combiner) through the MPDD MIMO channel can be mathematically modeled as follows:

$$\begin{aligned} \mathbf{r}(t) &\triangleq \mathbf{U}^H \mathbf{H}(\mathbf{Z}, \tilde{\mathbf{Z}}, \mathcal{F}, t, \tau) * \mathbf{V} \mathbf{s}(t) + \mathbf{w}(t) \\ &= \int_{-\infty}^{\infty} \mathbf{U}^H \Upsilon_R(\tilde{\mathbf{Z}}) \mathbf{R}_{\text{RX}}^{1/2} \left[\tilde{\mathbf{H}}_d(t, \tau) + \sum_{k=1}^K \tilde{\mathbf{H}}_{\text{RX},k}(t, \tau) \Phi_k \tilde{\mathbf{H}}_{k,\text{TX}}(t, \tau) \right] \mathbf{R}_{\text{TX}}^{1/2} \Upsilon_T(\mathbf{Z}) \mathbf{V} \mathbf{s}(t - \tau) d\tau, \end{aligned} \quad (21)$$

where $\mathbf{w}(t) \triangleq \mathbf{U}^H \mathbf{n}(t) \in \mathbb{C}^{d_s \times 1}$ (omitted in the second inequality to avoid repetition) and $\mathbf{n}(t) \in \mathbb{C}^{N_R \times 1}$ denotes the additive white Gaussian noise (AWGN) vector at the RX side with spatially and temporally uncorrelated elements, each with zero mean and variance σ_n^2 .

Let $\mathbf{r}[n] \in \mathbb{C}^{d_s \times 1}$ and $\mathbf{s}[n] \in \mathbb{C}^{d_s \times 1}$, with $n \in \{0, \dots, N-1\}$, be the finite sequences obtained after respectively sampling $\mathbf{r}(t)$ and $\mathbf{s}(t)$ at a sufficiently high sampling rate [72] $F_S \triangleq \frac{1}{T_S}$ in Hz within a total bandwidth B . Then, the discrete-time equivalent of the received signal in expression (21) can be obtained as follows:

$$\begin{aligned} \mathbf{r}[n] &= \sum_{\ell=0}^{\infty} \left[\underbrace{\left(\sum_{k=1}^K \sum_{\bar{p}=1}^{\bar{P}} \sum_{\hat{p}=1}^{\hat{P}} J \sqrt{\frac{\bar{M}\hat{M}}{\bar{P}\hat{P}}} h_{\bar{p},k} h_{\hat{p},k} \mathbf{U}^H \Upsilon_R(\tilde{\mathbf{Z}}) \mathbf{R}_{\text{RX}}^{1/2} \mathbf{B}_{\bar{p},k} \Phi_k \mathbf{B}_{\hat{p},k} \mathbf{R}_{\text{TX}}^{1/2} \Upsilon_T(\mathbf{Z}) \mathbf{V}} \right)}_{\triangleq \check{\mathbf{H}}_{k,\bar{p},\hat{p}}^{\text{RIS}}(\mathbf{Z}, \tilde{\mathbf{Z}}, \Phi_k, \mathbf{V}, \mathbf{U}) \in \mathbb{C}^{d_s \times d_s}} \right. \\ &\quad \times e^{j2\pi \frac{n}{N} (f_{\bar{p},k} + f_{\hat{p},k})} \delta[\ell - (\ell_{\bar{p},k} + \ell_{\hat{p},k})] \\ &\quad \left. + \sum_{p=1}^P \underbrace{\left(\sqrt{\frac{\bar{M}\hat{M}}{P}} h_p \mathbf{U}^H \Upsilon_R(\tilde{\mathbf{Z}}) \mathbf{R}_{\text{RX}}^{1/2} \mathbf{B}_p \mathbf{R}_{\text{TX}}^{1/2} \Upsilon_T(\mathbf{Z}) \mathbf{V} e^{j2\pi f_p \frac{n}{N}} \delta[\ell - \ell_p] \right)}_{\triangleq \check{\mathbf{H}}_p^d(\mathbf{Z}, \tilde{\mathbf{Z}}, \mathbf{V}, \mathbf{U}) \in \mathbb{C}^{d_s \times d_s}} \right] \mathbf{s}[n - \ell] + \mathbf{w}[n], \end{aligned} \quad (22)$$

where ℓ indicates the normalized discrete delay index, while $f_p \triangleq \frac{N\nu_p}{F_S}$ and $\ell_p \triangleq \frac{\tau_p}{T_S}$ are respectively the normalized Doppler shift and the associated normalized discrete delay index of each p -th path propagation path between the TX-SIM and RX-SIM, with the definitions of $f_{\bar{p},k}$, $f_{\hat{p},k}$, $\ell_{\bar{p},k}$, and $\ell_{\hat{p},k}$ being similar for the respective channel paths.

By taking into account a cyclic prefix (CP) of length N_{CP} and utilizing the circular convolution, the N -element discrete-time received signal in (22) can be re-expressed as follows [8]:

$$\begin{aligned}
\mathbf{r}_v &= \sum_{u=1}^{d_s} \underbrace{\left(\sum_{p=1}^P \check{h}_{p,v,u}^d \underbrace{\mathbf{\Theta}_p \mathbf{\Omega}^{f_p} \mathbf{\Pi}^{\ell_p}}_{\triangleq \mathbf{G}_p \in \mathbb{C}^{N \times N}} + \sum_{k=1}^K \sum_{\bar{p}=1}^{\bar{P}} \sum_{\tilde{p}=1}^{\tilde{P}} \check{h}_{k,\bar{p},\tilde{p},v,u}^{\text{RIS}} \underbrace{\mathbf{\Theta}_{k,\bar{p},\tilde{p}} \mathbf{\Omega}^{f_{k,\bar{p},\tilde{p}}} \mathbf{\Pi}^{\ell_{k,\bar{p},\tilde{p}}}}_{\triangleq \mathbf{G}_{k,\bar{p},\tilde{p}} \in \mathbb{C}^{N \times N}} \right)}_{\triangleq \tilde{\mathbf{H}}_{v,u}^{\text{RIS}}(\mathcal{Z}, \tilde{\mathcal{Z}}, \mathcal{F}, \mathbf{V}, \mathbf{U}) \in \mathbb{C}^{N \times N}} \mathbf{s}_u + \mathbf{w}_v \\
&= \sum_{u=1}^{d_s} \underbrace{\left(\tilde{\mathbf{H}}_{v,u}^d(\mathcal{Z}, \tilde{\mathcal{Z}}, \mathbf{V}, \mathbf{U}) + \tilde{\mathbf{H}}_{v,u}^{\text{RIS}}(\mathcal{Z}, \tilde{\mathcal{Z}}, \mathcal{F}, \mathbf{V}, \mathbf{U}) \right)}_{\triangleq \tilde{\mathbf{H}}_{v,u}^{\text{tot}}(\mathcal{Z}, \tilde{\mathcal{Z}}, \mathcal{F}, \mathbf{V}, \mathbf{U}) \in \mathbb{C}^{N \times N}} \mathbf{s}_u + \mathbf{w}_v, \tag{23}
\end{aligned}$$

where, for notational simplicity, the discrete-time index is omitted (also henceforth), which is implied.

In expression (23), the scalars $\check{h}_{p,v,u}^d$ and $\check{h}_{k,\bar{p},\tilde{p},v,u}^{\text{RIS}}$, with $(v, u) = \{1, \dots, d_s\}$, are the (v, u) -th elements of the matrices $\check{\mathbf{H}}_p^d(\mathcal{Z}, \tilde{\mathcal{Z}}, \mathbf{V}, \mathbf{U})$ and $\check{\mathbf{H}}_{k,\bar{p},\tilde{p}}^{\text{RIS}}(\mathcal{Z}, \tilde{\mathcal{Z}}, \mathbf{\Phi}_k, \mathbf{V}, \mathbf{U})$, respectively, which are both implicitly defined in expression (22). In addition, $\mathbf{s}_u \triangleq [s_u[0], \dots, s_u[N-1]] \in \mathbb{C}^{N \times 1}$ and $\mathbf{w}_v \triangleq [w_v[0], \dots, w_v[N-1]] \in \mathbb{C}^{N \times 1}$ are the transmit signal and AWGN vectors for the u -th and v -th stream, respectively. In turn, each diagonal matrix $\mathbf{\Theta}_p \in \mathbb{C}^{N \times N}$ is defined as follows:

$$\mathbf{\Theta}_p \triangleq \text{diag} \left(\underbrace{[e^{-j2\pi\phi_{\text{CP}}(\ell_p)}, e^{-j2\pi\phi_{\text{CP}}(\ell_p-1)}, \dots, e^{-j2\pi\phi_{\text{CP}}(2)}, e^{-j2\pi\phi_{\text{CP}}(1)}]}_{\ell_p \text{ terms}}, \underbrace{[1, \dots, 1]}_{N-\ell_p \text{ ones}} \right), \tag{24}$$

capturing the effect of the CP onto the p -th channel path, with $\phi_{\text{CP}}(n)$ being a function of the sample index $n \in \{0, \dots, N-1\}$, representing a phase that depends on the specific waveform used. In addition, the diagonal matrix⁴ $\mathbf{\Omega} \in \mathbb{C}^{N \times N}$ given by

$$\mathbf{\Omega} \triangleq \text{diag} \left([1, e^{-j2\pi/N}, \dots, e^{-j2\pi(N-2)/N}, e^{-j2\pi(N-1)/N}] \right) \in \mathbb{C}^{N \times N} \tag{25}$$

contains the N complex roots of unity, while $\mathbf{\Pi} \in \{0, 1\}^{N \times N}$ is the forward cyclic shift matrix with elements defined as⁵

$$\pi_{i,j} \triangleq \delta_{i,j+1} + \delta_{i,j-(N-1)} \quad \delta_{ij} \triangleq \begin{cases} 0 & \text{if } i \neq j \\ 1 & \text{if } i = j \end{cases}. \tag{26}$$

⁴ Matrix exponentiation amounts to an element-wise exponentiation for diagonal matrices.

⁵ The matrix $\mathbf{\Pi}$ is defined such that $\mathbf{A}\mathbf{\Pi}^{\ell_p}$, with $\ell_p \in \mathbb{N}$, is a cyclic left-shifted version of \mathbf{A} , *i.e.*, the first ℓ_p columns of \mathbf{A} are moved to the positions of the last ℓ_p columns. It can be also seen that $\mathbf{\Pi}^0$ is the $N \times N$ identity matrix, yielding $\mathbf{A}\mathbf{\Pi}^0 = \mathbf{A}$.

Leveraging the Kronecker product to concatenate all d_s \mathbf{r}_v vectors in expression (23), the following Nd_s -element vector for the overall received signal in the TD, considering an arbitrary modulated transmit signal, is obtained:

$$\mathbf{r}_{\text{TD}} = \bar{\mathbf{H}}(\mathcal{Z}, \tilde{\mathcal{Z}}, \mathcal{F}, \mathbf{V}, \mathbf{U})\mathbf{s}_{\text{TD}} + \bar{\mathbf{w}}_{\text{TD}}, \quad (27)$$

where $\bar{\mathbf{H}}(\mathcal{Z}, \tilde{\mathcal{Z}}, \mathcal{F}, \mathbf{V}, \mathbf{U}) \in \mathbb{C}^{Nd_s \times Nd_s}$ explicitly highlights the dependence of the TD transfer function of the considered point-to-point MIMO system on the TX and RX SIM, the K RISs of the programmable smart wireless propagation environment, and the digital TX and RX beamformers, and is mathematically defined as follows:

$$\begin{aligned} \bar{\mathbf{H}}(\mathcal{Z}, \tilde{\mathcal{Z}}, \mathcal{F}, \mathbf{V}, \mathbf{U}) \triangleq & \sum_{p=1}^P (\check{\mathbf{H}}_p^d(\mathcal{Z}, \tilde{\mathcal{Z}}, \mathbf{V}, \mathbf{U}) \otimes \mathbf{G}_p) \\ & + \sum_{k=1}^K \sum_{\bar{p}=1}^{\bar{P}} \sum_{\tilde{p}=1}^{\tilde{P}} (\check{\mathbf{H}}_{k,\bar{p},\tilde{p}}^{\text{RIS}}(\mathcal{Z}, \tilde{\mathcal{Z}}, \Phi_k, \mathbf{V}, \mathbf{U}) \otimes \mathbf{G}_{k,\bar{p},\tilde{p}}), \end{aligned} \quad (28)$$

with the Nd_s -element vectors \mathbf{s}_{TD} and $\bar{\mathbf{w}}_{\text{TD}}$ resulting from the concatenation of \mathbf{s}_u 's and \mathbf{w}_v 's in (23), respectively. For notational simplicity, the matrices $\check{\mathbf{H}}_p^d$ and $\check{\mathbf{H}}_{k,\bar{p},\tilde{p}}^{\text{RIS}}$ appearing in equation (28) will hereafter be expressed without explicitly indicating their dependence on the TX/RX beamforming (BF) and SIM/RISs parameters.

4.2 OFDM Signaling

Let \mathcal{C} denote an arbitrary complex constellation set of cardinality D and average energy E_s , which is associated with a given digital modulation scheme (e.g., quadrature amplitude modulation (QAM)). In OFDM, multiple information vectors $\mathbf{x}_u \in \mathbb{C}^{N \times 1}$ with $u = \{1, \dots, d_s\}$, containing a total of Nd_s symbols, are modulated into the following transmit signal:

$$\mathbf{s}_u^{(\text{OFDM})} \triangleq \mathbf{F}_N^H \mathbf{x}_u \in \mathbb{C}^{N \times 1}, \quad (29)$$

where \mathbf{F}_N denotes the N -point normalized DFT matrix.

After undergoing circular convolution with the DD channel and using a formulation similar to expression (27), the corresponding Nd_s -element discrete-time received OFDM signal can be written as

$$\mathbf{r}_{\text{OFDM}} \triangleq \bar{\mathbf{H}}(\mathcal{Z}, \tilde{\mathcal{Z}}, \mathcal{F}, \mathbf{V}, \mathbf{U})\mathbf{s}_{\text{OFDM}} + \bar{\mathbf{w}}_{\text{TD}}, \quad (30)$$

where the Nd_s -element vectors are defined as

$$\mathbf{s}_{\text{OFDM}} \triangleq \begin{bmatrix} \mathbf{s}_1^{(\text{OFDM})} \\ \vdots \\ \mathbf{s}_{d_s}^{(\text{OFDM})} \end{bmatrix}, \quad \mathbf{r}_{\text{OFDM}} \triangleq \begin{bmatrix} \mathbf{r}_1^{(\text{OFDM})} \\ \vdots \\ \mathbf{r}_{d_s}^{(\text{OFDM})} \end{bmatrix}. \quad (31)$$

At the RX side, applying OFDM demodulation yields

$$\mathbf{y}_v^{(\text{OFDM})} \triangleq \mathbf{F}_N \mathbf{r}_v^{(\text{OFDM})} \in \mathbb{C}^{N \times 1}, \quad (32)$$

yielding the corresponding Nd_s -element discrete-time signal

$$\mathbf{y}_{\text{OFDM}} = \tilde{\mathbf{H}}_{\text{OFDM}}(\mathcal{Z}, \tilde{\mathcal{Z}}, \mathcal{F}, \mathbf{V}, \mathbf{U}) \mathbf{x} + \tilde{\mathbf{w}}_{\text{OFDM}}, \quad (33)$$

where $\tilde{\mathbf{w}}_{\text{OFDM}} \in \mathbb{C}^{Nd_s \times 1}$ is an equivalent AWGN with the same statistics as $\tilde{\mathbf{w}}_{\text{TD}}$, and $\tilde{\mathbf{H}}_{\text{OFDM}}(\mathcal{Z}, \tilde{\mathcal{Z}}, \mathcal{F}, \mathbf{V}, \mathbf{U}) \in \mathbb{C}^{Nd_s \times Nd_s}$ represents the effective OFDM channel defined similar to $\tilde{\mathbf{H}}(\mathcal{Z}, \tilde{\mathcal{Z}}, \mathcal{F}, \mathbf{V}, \mathbf{U})$ in (27), which is expressed as

$$\begin{aligned} \tilde{\mathbf{H}}_{\text{OFDM}} &\triangleq \sum_{p=1}^P \check{\mathbf{H}}_p^d \otimes \overbrace{(\mathbf{F}_N \mathbf{G}_p \mathbf{F}_N^H)}^{\triangleq \mathbf{G}_p^{\text{OFDM}} \in \mathbb{C}^{N \times N}} + \sum_{k=1}^K \sum_{\bar{p}=1}^{\bar{P}} \sum_{\tilde{p}=1}^{\tilde{P}} \check{\mathbf{H}}_{k,\bar{p},\tilde{p}}^{\text{RIS}} \otimes \overbrace{(\mathbf{F}_N \mathbf{G}_{k,\bar{p},\tilde{p}} \mathbf{F}_N^H)}^{\triangleq \mathbf{G}_{k,\bar{p},\tilde{p}}^{\text{OFDM}} \in \mathbb{C}^{N \times N}} \\ &= \sum_{p=1}^P \check{\mathbf{H}}_p^d \otimes \mathbf{G}_p^{\text{OFDM}} + \sum_{k=1}^K \sum_{\bar{p}=1}^{\bar{P}} \sum_{\tilde{p}=1}^{\tilde{P}} \check{\mathbf{H}}_{k,\bar{p},\tilde{p}}^{\text{RIS}} \otimes \mathbf{G}_{k,\bar{p},\tilde{p}}^{\text{OFDM}}. \end{aligned} \quad (34)$$

Notice that, for this OFDM case, the CP phase matrices Θ_p 's appearing in (23) reduce to identity matrices [8], i.e., $\phi_{\text{CP}}(n) = 0$ in (24), since there is no phase offset.

4.3 OTFS Signaling

When OTFS is used, multiple matrices $\mathbf{X}_u \in \mathbb{C}^{\tilde{K} \times \tilde{K}'}$ with $u = \{1, \dots, d_s\}$, containing a total of $\tilde{K} \tilde{K}' d_s$ symbols taken from an arbitrary complex constellation \mathcal{C} , are modulated as follows⁶:

$$\mathbf{s}_u^{(\text{OTFS})} \triangleq \text{vec}(\mathbf{S}_u) = (\mathbf{F}_{\tilde{K}'}^H \otimes \mathbf{I}_{\tilde{K}}) \text{vec}(\mathbf{X}_u) \in \mathbb{C}^{\tilde{K} \tilde{K}' \times 1}, \quad (35)$$

where $\text{vec}(\cdot)$ denotes matrix vectorization via column stacking and \mathbf{S}_u is a TD symbols' matrix obtained from⁷ the inverse discrete Zak transform (IDZT) of \mathbf{X}_u as follows [73]:

$$\mathbf{S}_u = \mathbf{X}_u \mathbf{F}_{\tilde{K}'}^H \in \mathbb{C}^{\tilde{K} \times \tilde{K}'}. \quad (36)$$

The notation in (35) is in line with the strategy described in [74], whereby the OTFS signals are first vectorized and then appended with a CP of length N_{CP} in order to eliminate inter-frame interference, in similarity with OFDM. Taking advantage of this similarity, and in order to allow for direct comparisons between the two waveforms, $\tilde{K} \times \tilde{K}' = N$ is set hereafter.

⁶ For simplicity, all pulse-shaping operations are assumed to utilize rectangular waveforms such that the corresponding sample matrices can be reduced to identity matrices.

⁷ Equivalently, \mathbf{S}_u can be obtained as the Heisenberg transform of the inverse symplectic finite Fourier transform (ISFFT) of \mathbf{X}_u , i.e., $\mathbf{S}_u = \mathbf{F}_{\tilde{K}'}^H \mathbf{X}_{\text{FT}}^u$ with $\mathbf{X}_{\text{FT}}^u \triangleq \mathbf{F}_{\tilde{K}} \mathbf{X}_u \mathbf{F}_{\tilde{K}'}^H \in \mathbb{C}^{\tilde{K} \times \tilde{K}'}$.

After transmission over the DD channel $\tilde{\mathbf{H}}(\mathcal{Z}, \tilde{\mathcal{Z}}, \mathcal{F}, \mathbf{V}, \mathbf{U})$ as shown in expression (27), the Nd_s -element discrete-time received OTFS signal can be modeled similar to (30) as $\mathbf{r}_{\text{OTFS}} \triangleq \tilde{\mathbf{H}}(\mathcal{Z}, \tilde{\mathcal{Z}}, \mathcal{F}, \mathbf{V}, \mathbf{U})\mathbf{s}_{\text{OTFS}} + \tilde{\mathbf{w}}_{\text{TD}}$, where the Nd_s -element vectors \mathbf{s}_{OTFS} and \mathbf{r}_{OTFS} are defined for OTFS similar to expression (31). However, unlike OFDM, the detection of the information symbols \mathbf{X}_u 's from the $\mathbf{r}_v^{(\text{OTFS})}$ elements $\forall v = 1, \dots, d_s$ of \mathbf{r}_{OTFS} requires reversing the vectorization and the IDZT operations employed in the construction of the d_s elements of \mathbf{s}_{OTFS} , resulting in a distinct effective channel. In particular, let $\mathbf{R}_v \triangleq \text{vec}^{-1}(\mathbf{r}_v^{(\text{OTFS})}) \in \mathbb{C}^{\tilde{K} \times \tilde{K}'}$, with $\text{vec}^{-1}(\cdot)$ indicating the de-vectorization operation according to which a vector of size $\tilde{K}\tilde{K}' \times 1$ is reshaped into a matrix of size $\tilde{K} \times \tilde{K}'$, and consider the following discrete Zak transform (DZT)⁸

$$\mathbf{Y}_v = \mathbf{R}_v \mathbf{F}_{\tilde{K}'} \in \mathbb{C}^{\tilde{K} \times \tilde{K}'}. \quad (37)$$

The demodulated OTFS signal at the RX then becomes

$$\mathbf{y}_v^{(\text{OTFS})} \triangleq \text{vec}(\mathbf{Y}_v) = (\mathbf{F}_{\tilde{K}'} \otimes \mathbf{I}_{\tilde{K}'}) \mathbf{r}_v^{(\text{OTFS})} \in \mathbb{C}^{N \times 1}, \quad (38)$$

which can be compactly written, similar to (33), as the following Nd_s -element discrete-time received signal:

$$\bar{\mathbf{y}}_{\text{OTFS}} = \tilde{\mathbf{H}}_{\text{OTFS}}(\mathcal{Z}, \tilde{\mathcal{Z}}, \mathcal{F}, \mathbf{V}, \mathbf{U})\mathbf{x} + \tilde{\mathbf{w}}_{\text{OTFS}}, \quad (39)$$

where $\tilde{\mathbf{w}}_{\text{OTFS}} \in \mathbb{C}^{Nd_s \times 1}$ is an equivalent AWGN with the same statistics as $\tilde{\mathbf{w}}_{\text{TD}}$, while $\tilde{\mathbf{H}}_{\text{OTFS}}(\mathcal{Z}, \tilde{\mathcal{Z}}, \mathcal{F}, \mathbf{V}, \mathbf{U}) \in \mathbb{C}^{Nd_s \times Nd_s}$ represents the effective OTFS channel and is given by

$$\begin{aligned} \tilde{\mathbf{H}}_{\text{OTFS}} &\triangleq \sum_{p=1}^P \check{\mathbf{H}}_p^d \otimes \overbrace{((\mathbf{F}_{\tilde{K}'} \otimes \mathbf{I}_{\tilde{K}'}) \mathbf{G}_p (\mathbf{F}_{\tilde{K}'}^H \otimes \mathbf{I}_{\tilde{K}'}))}^{\triangleq \mathbf{G}_p^{\text{OTFS}} \in \mathbb{C}^{N \times N}} \\ &+ \sum_{k=1}^K \sum_{\tilde{p}=1}^{\tilde{P}} \check{\mathbf{H}}_{k, \tilde{p}}^{\text{RIS}} \otimes \overbrace{((\mathbf{F}_{\tilde{K}'} \otimes \mathbf{I}_{\tilde{K}'}) \mathbf{G}_{k, \tilde{p}, \tilde{p}} (\mathbf{F}_{\tilde{K}'}^H \otimes \mathbf{I}_{\tilde{K}'}))}^{\triangleq \mathbf{G}_{k, \tilde{p}, \tilde{p}}^{\text{OTFS}} \in \mathbb{C}^{N \times N}} \\ &= \sum_{p=1}^P \check{\mathbf{H}}_p^d \otimes \mathbf{G}_p^{\text{OTFS}} + \sum_{k=1}^K \sum_{\tilde{p}=1}^{\tilde{P}} \check{\mathbf{H}}_{k, \tilde{p}}^{\text{RIS}} \otimes \mathbf{G}_{k, \tilde{p}, \tilde{p}}^{\text{OTFS}}. \end{aligned} \quad (40)$$

Notice that similarly to the OFDM case, the CP phase matrices Θ_p 's reduce to identity matrices [8]. Comparing the expressions in (34) and (40), one can appreciate how [8]'s channel modeling approach elucidates both the similarity in form as well

⁸ Equivalently, \mathbf{Y}_v can be obtained as the SFFT of the Wigner transform of \mathbf{R}_v : $\mathbf{Y}_{\text{FT}}^v \triangleq \mathbf{F}_{\tilde{K}'} \mathbf{R}_v$, yielding $\mathbf{Y}_v = \mathbf{F}_{\tilde{K}'}^H \mathbf{Y}_{\text{FT}}^v \in \mathbb{C}^{\tilde{K} \times \tilde{K}'}$.

as the distinction in effect between the OFDM and OTFS waveforms in DD channels, even under artificial enhancements such as the RISs and SIM.

4.4 AFDM Signaling

The signal for transmission per information vector \mathbf{x}_u when AFDM waveform is used for the considered DD MIMO channel is given by the inverse discrete affine Fourier transform (IDAFT), as follows

$$\mathbf{s}_u^{(\text{AFDM})} \triangleq \mathbf{\Lambda}_1^H \mathbf{F}_N^H \mathbf{\Lambda}_2^H \mathbf{x}_u \in \mathbb{C}^{N \times 1}, \quad (41)$$

where the $N \times N$ matrices $\mathbf{\Lambda}_i$, with $i = 1, 2$, are defined as

$$\mathbf{\Lambda}_i \triangleq \text{diag}([1, e^{-j2\pi c_i 2^2}, \dots, e^{-j2\pi c_i (N-1)^2}]), \quad (42)$$

where the first central chirp frequency c_1 is an optimally designed parameter based on the maximum Doppler channel statistics [34, 8], while the second central chirp frequency c_2 is relatively a free parameter that can be exploited for ISAC waveform shaping [75] or information encoding [76, 35].

It was shown in [8] that, after going through a DD channel, an AFDM modulated symbol vector $\mathbf{s}_u^{(\text{AFDM})}$ with the inclusion of a *chirp-periodic* prefix (CPP) can be modeled similar to (23), by replacing the CP matrix $\mathbf{\Theta}_p$ in expression (24) with the CPP matrix generated via setting the function $\phi_{\text{CP}}(n)$ in (24) to be $\phi_{\text{CP}}(n) = c_1(N^2 - 2Nn)$ [25]. To this end, the Nd_s -element discrete-time received AFDM signal can be modeled similar to (30) as $\mathbf{r}_{\text{AFDM}} \triangleq \tilde{\mathbf{H}}(\mathcal{Z}, \tilde{\mathcal{Z}}, \mathcal{F}, \mathbf{V}, \mathbf{U})\mathbf{s}_{\text{AFDM}} + \tilde{\mathbf{w}}_{\text{TD}}$, where the Nd_s -element vectors \mathbf{s}_{AFDM} and \mathbf{r}_{AFDM} are defined for AFDM as in (31).

The AFDM demodulation of each of the $\mathbf{r}_v^{(\text{AFDM})}$ with $v \in \{1, \dots, d_s\}$ elements of \mathbf{r}_{AFDM} is obtained as

$$\mathbf{y}_v^{(\text{AFDM})} = \mathbf{\Lambda}_2 \mathbf{F}_N \mathbf{\Lambda}_1 \mathbf{r}_v^{(\text{AFDM})} \in \mathbb{C}^{N \times 1}, \quad (39)$$

yielding the following expression for the Nd_s -element discrete-time received signal (similar to expressions (33) and (39)):

$$\mathbf{y}_{\text{AFDM}} = \tilde{\mathbf{H}}_{\text{AFDM}}(\mathcal{Z}, \tilde{\mathcal{Z}}, \mathcal{F}, \mathbf{V}, \mathbf{U})\mathbf{x} + \tilde{\mathbf{w}}_{\text{AFDM}}, \quad (40)$$

where $\tilde{\mathbf{w}}_{\text{AFDM}} \in \mathbb{C}^{Nd_s \times 1}$ is an equivalent AWGN holding the same statistics with $\tilde{\mathbf{w}}_{\text{TD}}$, and $\tilde{\mathbf{H}}_{\text{AFDM}}(\mathcal{Z}, \tilde{\mathcal{Z}}, \mathcal{F}, \mathbf{V}, \mathbf{U}) \in \mathbb{C}^{Nd_s \times Nd_s}$ indicates the effective AFDM channel given by

$$\begin{aligned}
\bar{\mathbf{H}}_{\text{AFDM}} &\triangleq \sum_{p=1}^P \check{\mathbf{H}}_p^d \otimes \overbrace{(\Lambda_2 \mathbf{F}_N \Lambda_1 \mathbf{G}_p \Lambda_1^H \mathbf{F}_N^H \Lambda_2^H)}^{\mathbf{G}_p^{\text{AFDM}} \in \mathbb{C}^{N \times N}} \\
&+ \sum_{k=1}^K \sum_{\bar{p}=1}^{\bar{P}} \sum_{\tilde{p}=1}^{\tilde{P}} \check{\mathbf{H}}_{k,\bar{p},\tilde{p}}^{\text{RIS}} \otimes \overbrace{(\Lambda_2 \mathbf{F}_N \Lambda_1 \mathbf{G}_{k,\bar{p},\tilde{p}} \Lambda_1^H \mathbf{F}_N^H \Lambda_2^H)}^{\mathbf{G}_{k,\bar{p},\tilde{p}}^{\text{AFDM}} \in \mathbb{C}^{N \times N}} \\
&= \sum_{p=1}^P \check{\mathbf{H}}_p^d \otimes \mathbf{G}_p^{\text{AFDM}} + \sum_{k=1}^K \sum_{\bar{p}=1}^{\bar{P}} \sum_{\tilde{p}=1}^{\tilde{P}} \check{\mathbf{H}}_{k,\bar{p},\tilde{p}}^{\text{RIS}} \otimes \mathbf{G}_{k,\bar{p},\tilde{p}}^{\text{AFDM}}. \quad (41)
\end{aligned}$$

Clearly, the latter expression has the same structure of both (34) and (40), with the same holding for the MIMO input-output relationships described by expressions (33), (39), and (40). This implies that signal processing techniques such as channel estimation can be designed to under a unified framework, applying to OFDM, OTFS, AFDM, and similar waveforms.

Finally, for the sake of clarity, a ‘‘conventional’’ DD-MIMO model – *i.e.*, a MIMO extension of the model in [8] without the incorporation of RIS in the ambient and of the TX and RX SIM corresponding to the MIMO delay-time model defined in (7) in Section 2.1 – can be trivially extracted from the above. For instance, for the OFDM, OTFS, and AFDM waveforms, expressions (34), (40), and (41), would yield

$$\bar{\mathbf{H}}_{\text{MIMO}} \triangleq \sqrt{\frac{N_T N_R}{P}} \sum_{p=1}^P \left(h_p \mathbf{a}_R(\phi_p^{\text{in}}) \mathbf{a}_T^H(\phi_p^{\text{out}}) \right) \otimes \mathbf{G}_p^{\text{MIMO}}, \quad (42)$$

where the previous subscripts OFDM, OTFS, and AFDM, are respectively represented by the generic subscript MIMO.

4.5 Comparison of Effective Channels

As an example of how the aforementioned waveforms are affected by a MPDD MIMO channel, consider a point-to-point system with $N_T = N_R = 4$ antennas, such that up to $d_s = 4$ independent data streams can be utilized. Assume that the system operates with a carrier frequency of 28 GHz (*i.e.*, at wavelength $\lambda = 10.7$ mm) with a bandwidth $B = 20$ MHz in an environment with identical TX and RX SIM, both with $Q = \tilde{Q} = 5$ layers of metasurfaces and $M = \tilde{M} = 100$ meta-atoms per layer, leading to $M_x = M_z = \tilde{M}_x = \tilde{M}_z = 10$. In line with the Rayleigh-Sommerfeld diffraction theory, the distance between any two adjacent metasurface layers at either the TX or RX is 5λ , while the distance between two adjacent meta-atoms on any layer is $\lambda/2$ both along the x - and z -axis, such that $\rho_t = \rho_r = \lambda^2/4$. The assumptions that the SIMs are unoptimized and that the environment lacks any RIS presence are also adopted, thus, we set $\mathcal{Z} = \tilde{\mathcal{Z}} = \mathcal{F} = \mathbf{I}_{M/\tilde{M}/J} \forall q, \tilde{q}, k$.

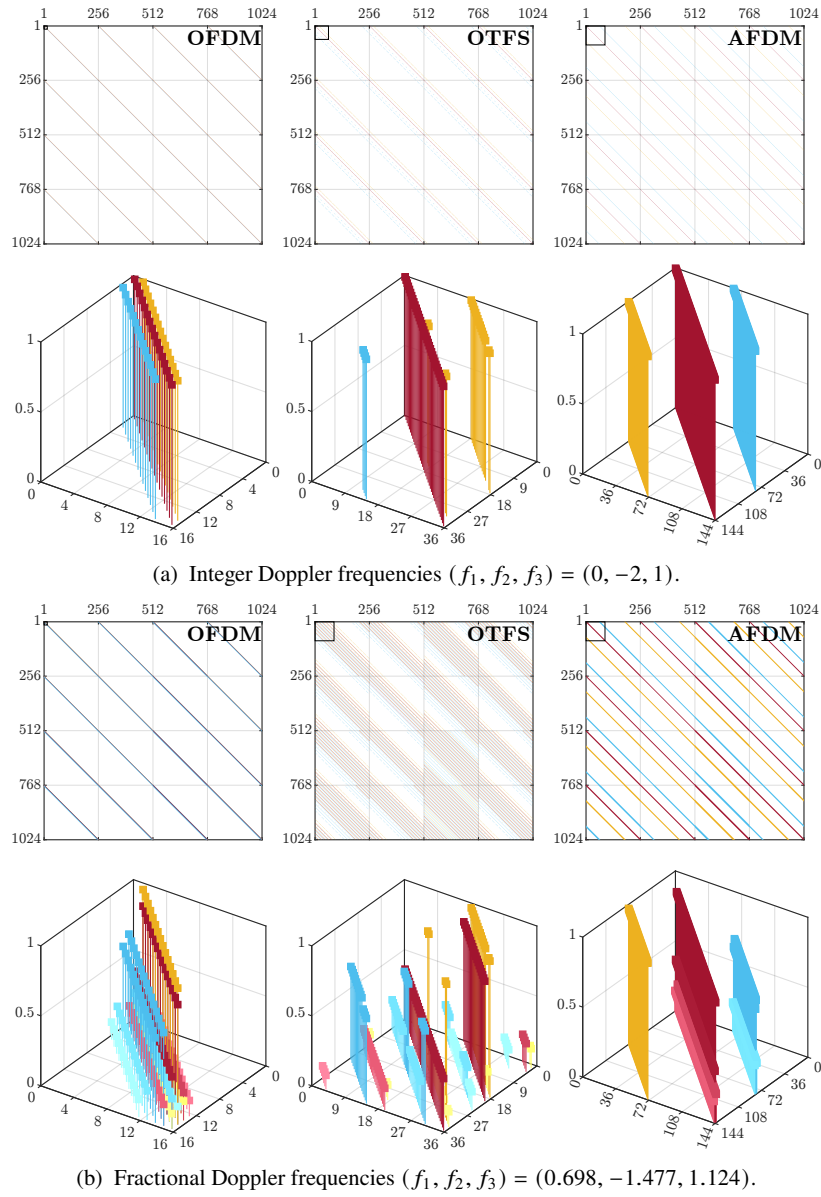


Fig. 2: Unoptimized 4×4 MPDD-MIMO with identical TX and RX SIM with $Q = \tilde{Q} = 5$ layers and $M = \tilde{M} = 100$ meta-atoms per layer, considering OFDM, OTFS, and AFDM with $N = 256$ symbols per frame and $P = 3$ channel paths with respective delays $(\ell_1, \ell_2, \ell_3) = (0, 5, 14)$ and integer (figure a) as well as fractional (figure b) Doppler frequencies. The 3D versions show the amplitude of the channel taps corresponding to the carriers outlined by the squares of the upper left corners.

Since the ULAs are aligned with the meta-atoms on the SIM, the angle between the propagation and the normal direction of the metasurface layers becomes in this case $\epsilon_{m,m'}^q = \tilde{\epsilon}_{\tilde{m},\tilde{m}'}^{\tilde{q}} = 0 \forall q, \tilde{q}, m, \tilde{m}, m', \tilde{m}'$. Consequently, Ψ_q 's, Γ_q 's, Δ_q 's, and Ξ_q 's can be generated from expressions (9) and (10), leading to the generation of the transfer functions Υ_T and Υ_R for the TX and RX SIM, respectively, as given in (11) and (12), respectively.

The TX/RX digital beamformers are also unoptimized and set as $\mathbf{V} = \mathbf{U} = \mathbf{I}_{d_s}$. Finally, the sampling frequency is set to $F_S = B$ and the number of symbols per frame to $N = 256$. For the MPDD channel, the path delays τ_p 's are uniformly distributed in $[0, \tau_{\max}]$, and that the Doppler shifts follow a Jakes spectrum, *i.e.*, $\nu_p = \nu_{\max} \cos(\theta_p) \forall p$ with each θ_p uniformly distributed in $[-\pi, \pi]$. In turn, the 2D and three-dimensional (3D) elevation AoDs/AoAs are uniformly distributed in $[0, \pi]$, while the 3D azimuth AoDs/AoAs are in $[-\frac{\pi}{2}, \frac{\pi}{2}]$. Finally, the setup considers a case with $P = 3$ paths, with respective delays $[\ell_1, \ell_2, \ell_3] = [0, 5, 14]$.

Figure 2 illustrates the resulting unoptimized MPDD-MIMO channels with all considered waveforms. As observed from Fig. 2b, the fractional components of the Doppler shift “spread” the path-wise components, making the effective channel matrix design vital for estimation/detection tasks to avoid overlaps and mixing among paths. Comparing the results shown in Fig. 2 with those in [8], it can be confirmed that, as expected, unoptimized SIM have no effect onto the DD channels undergone by the compared OFDM, OTFS, and AFDM waveforms. In what follows, however, it is demonstrated that when optimized, these structures can significantly impact on the detection performance of such systems.

5 SIM Optimization and Data Detection

A great potential advantage of MIMO systems incorporating SIM, compared to conventional MIMO systems, is that signal processing functions previously carried out by circuitry, be it in analog or digital fashions, can instead be performed in the wave propagation domain [61, 66]. And while this new wave-domain processing capability can be exploited to replace classic digital/analog processing, as suggested *e.g.* in [59, 64], it can also be utilized to augment it. Focusing on the latter case, and to elaborate further, consider, for example the trade-off that exists between enhancing the signal-to-noise ratio (SNR) of received signals and improving communication rate [77], which from the viewpoint of receiver design translates to either designing directivity-enhancing receive beamformers (*i.e.*, combiners) or, instead, exploiting the multiple streams of data as extrinsic information for detection [78]. Under the conventional paradigm, a choice (or trade-off) between these competing interests must be made. In contrast, in the case of MIMO-SIM systems, one can seek to reap the best of both worlds, by parameterizing the SIM for SNR gain, while leaving the degrees of freedom afforded by the multiple RX antennas to design robust detectors.

With the latter approach in mind, this section offers an illustrative application of the channel model detailed above. In particular, an optimization problem that

leverages the reconfigurability of the proposed MPDD-MIMO model to increase the intensity of the complex channel coefficients at the electromagnetic (EM) domain is formulated, and subsequently, introduce a GaBP-based data detection algorithm that exploits the signals from all RX antennas simultaneously and extrinsically [65]. The flexibility of the model is highlighted by offering both of the aforementioned contributions in a manner that they apply to OFDM, OTFS and AFDM alike.

5.1 SIM-Based Signal Enhancement

Referring to expression (22), setting the BF matrices \mathbf{U} and \mathbf{V} to identities to put emphasis on the impact of SIM as per the discussion above, and considering for simplicity a scenario without any RIS, the goal is to parametrize the matrices \mathcal{Z} and $\tilde{\mathcal{Z}}$ to enhance the total receive signal power, which can be achieved by solving the following optimization problem:

$$\begin{aligned} \max_{\mathcal{Z}, \tilde{\mathcal{Z}}} O(\mathcal{Z}, \tilde{\mathcal{Z}}) &= \sum_{p=1}^P \left\| \overbrace{\tilde{h}_p \Upsilon_{\mathbf{R}}(\tilde{\mathcal{Z}}) \mathbf{R}_{\text{RX}}^{1/2} \mathbf{B}_p \mathbf{R}_{\text{TX}}^{1/2} \Upsilon_{\mathbf{T}}(\mathcal{Z})}^{\triangleq \mathbf{O}_p} \right\|_F^2 \\ \text{s.t. } \Upsilon_{\mathbf{T}}(\mathcal{Z}) &\text{ as in eq. (11), } \Upsilon_{\mathbf{R}}(\tilde{\mathcal{Z}}) \text{ as in eq. (12),} \\ \Psi_q &\text{ and } \Lambda_{\tilde{q}} \text{ as in eqs. (9) and (14), respectively,} \\ |\zeta_m^q| &\leq \pi \forall (q, m), \text{ and } |\tilde{\zeta}_{\tilde{m}}^{\tilde{q}}| \leq \pi \forall (\tilde{q}, \tilde{m}). \end{aligned} \quad (43)$$

Notice that the array response matrix \mathbf{B}_p corresponding to a p -th path, defined previously in (18), as well as the scalar \tilde{h}_p defined as $\tilde{h}_p \triangleq h_p \sqrt{\frac{M\tilde{M}}{P}}$ were used here.

In view of the non-convex unit modulus constraints in (43)'s optimization problem, a simple gradient ascent technique is utilized to tune the phase shift parameters of the SIM. In particular, following [85], the gradient ascent algorithm is employed to adjust the phase shifts of the transmit and receive SIM iteratively, maximizing the objective function in equation (43). The algorithm is divided into two main discrete steps, addressed in detailed below.

5.1.1 Gradient Calculation

The gradient of the objective function $O(\mathcal{Z}, \tilde{\mathcal{Z}})$ with respect to the phase shift vector of the q -th layer of the TX-SIM, denoted by $\zeta_q = [\zeta_1^q, \zeta_2^q, \dots, \zeta_M^q]^\top$, is given by the following expression $\forall q$:

$$\nabla_{\zeta_q} O(\mathcal{Z}, \tilde{\mathcal{Z}}) = \sum_{p=1}^P \sum_{n_t=1}^{N_T} \nabla_{\zeta_q} \|\mathbf{o}_{p, n_t}\|^2, \quad (44)$$

where $\mathbf{o}_{p,n_t} \in \mathbb{C}^{N_R \times 1}$, with $n_t = \{1, 2, \dots, N_T\}$ and $p = \{1, 2, \dots, P\}$, represents the n_t -th column of the p -th \mathbf{O}_p matrix defined within the objective function in problem (43). Similarly, the gradient with respect to the phase shift vector $\tilde{\zeta}_{\tilde{q}} = [\tilde{\zeta}_1^{\tilde{q}}, \tilde{\zeta}_2^{\tilde{q}}, \dots, \tilde{\zeta}_M^{\tilde{q}}]^T$ of the \tilde{q} -th layer of the RX-SIM is given by

$$\nabla_{\tilde{\zeta}_{\tilde{q}}} O(\mathcal{Z}, \tilde{\mathcal{Z}}) = \sum_{p=1}^P \sum_{n_t=1}^{N_T} \nabla_{\tilde{\zeta}_{\tilde{q}}} \|\mathbf{o}_{p,n_t}\|^2, \quad \forall \tilde{q}. \quad (45)$$

Leveraging the chain rule, the per-shift partial derivatives of $\|\mathbf{o}_{p,n_t}\|^2$ with respect to ζ_m^q are given as follows $\forall m, q$:

$$\begin{aligned} \frac{\partial \|\mathbf{o}_{p,n_t}\|^2}{\partial \zeta_m^q} &= 2\Re \left\{ \frac{\partial \mathbf{o}_{p,n_t}^H}{\partial \zeta_m^q} \mathbf{o}_{p,n_t} \right\} = 2\Re \left\{ \frac{\partial (\tilde{\mathbf{Y}}_{t:q,p,n_t} \text{vec}(\mathbf{\Psi}_q))^H}{\partial \zeta_m^q} \mathbf{o}_{p,n_t} \right\} \\ &= 2\Re \left\{ -J e^{-J\zeta_m^q} \mathbf{i}_m^T \tilde{\mathbf{Y}}_{t:q,p,n_t}^H \mathbf{o}_{p,n_t} \right\} = 2\Im \left\{ e^{-J\zeta_m^q} \mathbf{i}_m^T \tilde{\mathbf{Y}}_{t:q,p,n_t}^H \mathbf{o}_{p,n_t} \right\}, \end{aligned} \quad (46)$$

where \mathbf{i}_m stands for the m -th column of \mathbf{I}_M and the second equality holds due to the fact that $\mathbf{o}_{p,n_t} = \tilde{\mathbf{Y}}_{t:q,p,n_t} \text{vec}(\mathbf{\Psi}_q)$, with $\tilde{\mathbf{Y}}_{t:q,p,n_t} \in \mathbb{C}^{N_R \times M}$ denoting the equivalent channel matrix of the p -th path associated to the q -th layer of the TX-SIM and the n_t -th transmit antenna, which is defined as follows

$$\tilde{\mathbf{Y}}_{t:q,p,n_t} \triangleq \tilde{h}_p \mathbf{\Upsilon}_R(\tilde{\mathcal{Z}}) \mathbf{R}_{\text{RX}}^{1/2} \mathbf{B}_p \mathbf{R}_{\text{TX}}^{1/2} \prod_{q'=1}^{q+1} \mathbf{\Psi}_{Q-q'+1} \mathbf{\Gamma}_{Q-q'+1} \text{diag}(\mathbf{s}_{q,n_t}), \quad (47)$$

where $\mathbf{s}_{q,n_t} \in \mathbb{C}^{M \times 1}$ is the signal component activating the q -th layer of the TX-SIM associated to the n_t -th transmit antenna, which is defined as the n_t -th column of

$$\mathbf{S}_q = \mathbf{\Gamma}_q \prod_{q'=Q-q+2}^Q \mathbf{\Psi}_{Q-q'+1} \mathbf{\Gamma}_{Q-q'+1}. \quad (48)$$

Finally, the M partial derivatives of each p -th path can be gathered into a vector, yielding the following final expression for the gradient of the TX-SIM:

$$\nabla_{\zeta_q} O(\mathcal{Z}, \tilde{\mathcal{Z}}) = 2\Im \left\{ \sum_{p=1}^P \sum_{n_t=1}^{N_T} \mathbf{\Psi}_q^H \tilde{\mathbf{Y}}_{t:q,p,n_t}^H \mathbf{o}_{p,n_t} \right\}. \quad (49)$$

Similarly, considering the definition of the gradient for the RX-SIM in (45) and expressing the per-shift partial derivatives with respect to $\zeta_{\tilde{m}}^{\tilde{q}}$, yields $\forall \tilde{m}, \tilde{q}$:

$$\begin{aligned}
\frac{\partial \|\mathbf{o}_{p,n_t}\|^2}{\partial \zeta_{\tilde{m}}^{\tilde{q}}} &= 2\Re \left\{ \frac{\partial \mathbf{o}_{p,n_t}^H}{\partial \zeta_{\tilde{m}}^{\tilde{q}}} \mathbf{o}_{p,n_t} \right\} = 2\Re \left\{ \frac{\partial (\tilde{\mathbf{Y}}_{r:\tilde{q},p,n_t} \text{vec}(\tilde{\Delta}_{\tilde{q}}))^H}{\partial \zeta_{\tilde{m}}^{\tilde{q}}} \mathbf{o}_{p,n_t} \right\} \\
&= 2\Re \left\{ -J e^{-J\zeta_{\tilde{m}}^{\tilde{q}}} \mathbf{i}_{\tilde{m}}^T \tilde{\mathbf{Y}}_{r:\tilde{q},p,n_t}^H \mathbf{o}_{p,n_t} \right\} = 2\Im \left\{ e^{-J\zeta_{\tilde{m}}^{\tilde{q}}} \mathbf{i}_{\tilde{m}}^T \tilde{\mathbf{Y}}_{r:\tilde{q},p,n_t}^H \mathbf{o}_{p,n_t} \right\},
\end{aligned} \tag{50}$$

where $\mathbf{i}_{\tilde{m}}$ stands for the \tilde{m} -th column of $\mathbf{I}_{\tilde{M}}$ and the second equality holds due to $\mathbf{o}_{p,n_t} = \tilde{\mathbf{Y}}_{r:\tilde{q},p,n_t} \text{vec}(\tilde{\Delta}_{\tilde{q}})$, with $\tilde{\mathbf{Y}}_{r:\tilde{q},p,n_t} \in \mathbb{C}^{N_R \times \tilde{M}}$ denoting the equivalent channel matrix of the p -th path associated to the \tilde{q} -th layer of the RX-SIM and the n_t -th transmit antenna, which is defined as follows:

$$\tilde{\mathbf{Y}}_{r:\tilde{q},p,n_t} \triangleq \tilde{h}_p \Xi_1 \left(\prod_{\tilde{q}'=1}^{\tilde{q}-1} \Delta_{\tilde{q}'} \Xi_{\tilde{q}'+1} \right) \text{diag}(\tilde{\mathbf{s}}_{\tilde{q},n_t}). \tag{51}$$

In this expression, $\tilde{\mathbf{s}}_{\tilde{q},n_t} \in \mathbb{C}^{\tilde{M} \times 1}$ is the signal component activating the \tilde{q} -th layer of the RX-SIM associated to the n_t -th transmit antenna, which is defined as the n_t -th column of the following matrix:

$$\tilde{\mathbf{S}}_{\tilde{q}} = \left(\prod_{\tilde{q}'=\tilde{q}+1}^{\tilde{Q}} \Xi_{\tilde{q}'} \Delta_{\tilde{q}'} \right) \mathbf{R}_{\text{RX}}^{1/2} \mathbf{B}_p \mathbf{R}_{\text{TX}}^{1/2} \mathbf{r}_T(\mathcal{Z}). \tag{52}$$

Finally, the \tilde{M} partial derivatives of each p -th path can be gathered, giving the final calculation for the gradient of the TX-SIM as follows:

$$\nabla_{\tilde{\zeta}_{\tilde{q}}} O(\mathcal{Z}, \tilde{\mathcal{Z}}) = 2\Im \left\{ \sum_{p=1}^P \sum_{n_t=1}^{N_T} \Delta_{\tilde{q}}^H \tilde{\mathbf{Y}}_{r:\tilde{q},p,n_t}^H \mathbf{o}_{p,n_t} \right\}. \tag{53}$$

5.1.2 Parameter Update

With the aforementioned closed-form expressions for the gradient of $O(\mathcal{Z}, \tilde{\mathcal{Z}})$ with respect to the TX- and RX-SIM phase parameters given respectively by the expressions (49) and (53), the update required to iteratively adjust the phases ζ_q and $\tilde{\zeta}_{\tilde{q}}$ to optimize the total receive powers, as described in the optimization problem (43), can be efficiently computed by

$$\zeta_q^{(i+1)} = \zeta_q^{(i)} + \lambda^i \rho^{(i)} \nabla_{\zeta_q} O(\mathcal{Z}, \tilde{\mathcal{Z}}), \tag{54a}$$

$$\tilde{\zeta}_{\tilde{q}}^{(i+1)} = \tilde{\zeta}_{\tilde{q}}^{(i)} + \lambda^i \tilde{\rho}^{(i)} \nabla_{\tilde{\zeta}_{\tilde{q}}} O(\mathcal{Z}, \tilde{\mathcal{Z}}), \tag{54b}$$

where $\lambda \in (0, 1)$ is the decaying learning rate parameter to ensure convergence and $\rho^{(i)}, \tilde{\rho}^{(i)}$ are normalization parameters calculated at each step as follows:

$$\rho^{(i)} = \pi / \max_{q \in Q, m \in M} \nabla_{\zeta_q} \mathcal{O}(\mathcal{Z}, \tilde{\mathcal{Z}}), \quad (55a)$$

$$\tilde{\rho}^{(i)} = \pi / \max_{\tilde{q} \in \tilde{Q}, \tilde{m} \in \tilde{M}} \nabla_{\tilde{\zeta}_{\tilde{q}}} \mathcal{O}(\mathcal{Z}, \tilde{\mathcal{Z}}). \quad (55b)$$

5.2 GaBP-Based Data Detection

In possession of the SIM optimization method detailed above, and given the input-output relationships given in Section 4 for various exemplary ISAC-enabling waveforms, the impact of integrating SIM onto the design of communication systems under the MPDD-MIMO channel model described in Section 3 can be demonstrated, by comparing the corresponding performances of OFDM, OTFS and AFDM, with and without SIM.

Before proceeding, recall that it has been widely demonstrated [21, 25] that AFDM and OTFS can significantly outperform OFDM under DD conditions. It shall be demonstrated, however, that SIM can significantly lower the performance gap between these waveforms which in turn, given the potential of the technology to reduce hardware complexity compared to traditional digital signal processing techniques, suggests that the design of waveforms to combat DD distortion can be significantly impacted by the emergence of SIM.

From a receiver design viewpoint, the aim is to estimate the transmitted signal \mathbf{x} , under the assumption that the effective channel matrix $\tilde{\mathbf{H}}$ is known. In order to derive a GaBP-based detector for arbitrary waveforms, consider the following generic input-output (I/O) relationship:

$$\mathbf{y} = \tilde{\mathbf{H}}\mathbf{x} + \tilde{\mathbf{w}}, \quad (56)$$

where, for conciseness, the waveform specific subscripts are dropped from the notation of the effective channel matrix $\tilde{\mathbf{H}}$, which for OFDM, OTFS, and AFDM are respectively given by expressions (34), (40), and (41). By setting $\tilde{N} = \tilde{M} \triangleq Nd_s \times Nd_s$ with $\tilde{n} \triangleq \{1, \dots, \tilde{N}\}$ and $\tilde{m} \triangleq \{1, \dots, \tilde{M}\}$, the element-wise relationship corresponding to (56) is given by

$$y_{\tilde{n}} = \sum_{\tilde{m}=1}^{\tilde{M}} \tilde{h}_{\tilde{n}, \tilde{m}} x_{\tilde{m}} + \tilde{w}_{\tilde{n}}, \quad (57)$$

such that the soft replica of the \tilde{m} -th communication symbol associated with the \tilde{n} -th receive signal $y_{\tilde{n}}$, computed at the i -th iteration of a message-passing algorithm, can be denoted by $\hat{x}_{\tilde{n}, \tilde{m}}^{(i)}$, with the corresponding mean-squared-error (MSE) of these estimates computed for the i -th iteration as follows $\forall \tilde{n}, \tilde{m}$:

$$\hat{\sigma}_{x: \tilde{n}, \tilde{m}}^{2(i)} \triangleq \mathbb{E}_x [|x - \hat{x}_{\tilde{n}, \tilde{m}}^{(i-1)}|^2] = E_S - |\hat{x}_{\tilde{n}, \tilde{m}}^{(i-1)}|^2, \quad (58)$$

where \mathbb{E}_x refers to expectation over all the possible symbols in the constellation \mathcal{C} . The GaBP receiver for such a setup consists of three major stages, as described below.

5.2.1 Soft Interference Cancellation

The objective of the soft interference cancellation (soft IC) stage at a given i -th iteration of the algorithm is to utilize the soft replicas $\hat{x}_{\bar{n},\bar{m}}^{(i-1)}$ from a previous iteration in order to calculate the data-centric soft IC signals $\tilde{y}_{x:\bar{n},\bar{m}}^{(i)}$. Exploiting expression (57), the soft IC signals are given by

$$\tilde{y}_{x:\bar{n},\bar{m}}^{(i)} = y_{\bar{n}} - \sum_{e \neq \bar{m}} h_{\bar{n},e} \hat{x}_{\bar{n},e}^{(i)}, \quad (59)$$

$$= h_{\bar{n},\bar{m}} x_{\bar{m}} + \underbrace{\sum_{e \neq \bar{m}} h_{\bar{n},e} (x_e - \hat{x}_{\bar{n},e}^{(i)})}_{\text{interference + noise term}} + \bar{w}_{\bar{n}}. \quad (60)$$

Leveraging the scalar Gaussian approximation (SGA), the interference and noise terms in this expression can be approximated as Gaussian noise, such that the conditional probability density functions (PDFs) of the soft IC signals become

$$p_{\tilde{y}_{x:\bar{n},\bar{m}}^{(i)} | x_{\bar{m}}}(\tilde{y}_{x:\bar{n},\bar{m}}^{(i)} | x_{\bar{m}}) \propto \exp\left[-\frac{|\tilde{y}_{x:\bar{n},\bar{m}}^{(i)} - h_{\bar{n},\bar{m}} x_{\bar{m}}|^2}{\tilde{\sigma}_{x:\bar{n},\bar{m}}^{2(i)}}\right] \quad (61)$$

with their conditional variances expressed as follows:

$$\tilde{\sigma}_{x:\bar{n},\bar{m}}^{2(i)} = \sum_{e \neq \bar{m}} |h_{\bar{n},e}|^2 \hat{\sigma}_{x:\bar{n},e}^{2(i)} + \sigma_w^2. \quad (62)$$

5.2.2 Belief Generation

In the belief generation stage of the algorithm, the SGA is exploited under the assumptions that \bar{N} is a sufficiently large number and that the individual estimation errors in $\hat{x}_{\bar{n},\bar{m}}^{(i-1)}$ are independent, in order to generate initial estimates (a.k.a. beliefs) for all the data symbols. As a consequence of the SGA and with the conditional PDFs of (61), the following extrinsic PDFs are deduced:

$$\prod_{e \neq \bar{n}} p_{\tilde{y}_{x:e,\bar{m}}^{(i)} | x_{\bar{m}}}(\tilde{y}_{x:e,\bar{m}}^{(i)} | x_{\bar{m}}) \propto \exp\left[-\frac{(x_{\bar{m}} - \bar{x}_{\bar{n},\bar{m}}^{(i)})^2}{\bar{\sigma}_{x:\bar{n},\bar{m}}^{2(i)}}\right], \quad (63)$$

where the corresponding extrinsic means and variances are respectively defined as

Algorithm 1 SIM Optimization and Data Detection

Input: Receive signal vector $\mathbf{y} \in \mathbb{C}^{N \times 1}$, complex channel matrix $\bar{\mathbf{H}} \in \mathbb{C}^{N \times \bar{M}}$, number of GaBP iterations i_{\max} , number of gradient descent iterations i_{GD} , data constellation power E_S , noise variance σ_w^2 , and damping factor β_x .

Output: $\hat{\mathbf{x}}$

Initialization

- Set iteration counter to $i = 0$ and amplitudes $c_x = \sqrt{E_S/2}$.
 - Set initial data estimates to $\hat{x}_{\bar{n}, \bar{m}}^{(0)} = 0$ and corresponding variances to $\bar{\sigma}_{x:\bar{n}, \bar{m}}^{2(0)} = E_S \forall \bar{n}, \bar{m}$.
-

SIM Optimization via Steepest Ascent

for $i = 1$ to i_{GD} **do**: $\forall q, \bar{q}, m, \bar{m}$

- 1: Compute the gradients from expressions (49) and (53).
- 2: Update normalization parameters from expression (55).
- 3: Update the phase parameters via expression (54).

end for

Data Detection via GaBP

for $i = 1$ to i_{\max} **do** $\forall \bar{n}, \bar{m}$

- 4: Compute soft IC data signal $\tilde{y}_{x:\bar{n}, \bar{m}}^{(i)}$ and its corresponding variance $\bar{\sigma}_{x:\bar{n}, \bar{m}}^{2(i)}$ from (59) and (62).
- 5: Compute extrinsic data signal belief $\bar{x}_{\bar{n}, \bar{m}}^{(i)}$ and its corresponding variance $\bar{\sigma}_{x:\bar{n}, \bar{m}}^{2(i)}$ from (64) and (65).
- 6: Compute denoised and damped data signal estimate $\hat{x}_{\bar{n}, \bar{m}}^{(i)}$ from (66) and (67).
- 7: Compute denoised and damped data signal variance $\bar{\sigma}_{x:\bar{n}, \bar{m}}^{2(i)}$ from (58) and (68).

end for

- 8: Calculate $\hat{x}_{\bar{m}} \forall \bar{m}$ (equivalently $\hat{\mathbf{x}}$) using (69).
-

$$\bar{x}_{\bar{n}, \bar{m}}^{(i)} = \bar{\sigma}_{x:\bar{n}, \bar{m}}^{(i)} \sum_{e \neq \bar{n}} \frac{h_{e, \bar{m}}^* \tilde{y}_{x:e, \bar{m}}^{(i)}}{\bar{\sigma}_{x:e, \bar{m}}^{2(i)}}, \quad (64)$$

$$\bar{\sigma}_{x:\bar{n}, \bar{m}}^{2(i)} = \left(\sum_{e \neq \bar{n}} \frac{|h_{e, \bar{m}}|^2}{\bar{\sigma}_{x:e, \bar{m}}^{2(i)}} \right)^{-1}. \quad (65)$$

with $h_{e, \bar{m}}^*$ denoting the complex conjugate of $h_{e, \bar{m}}$.

5.2.3 Soft Replica Generation

Finally, the soft replica generation stage consists of denoising the previously computed beliefs under a Bayes-optimal rule, in order to obtain the final estimates for the desired variables. For quadrature phase-shift keying (QPSK) modulation⁹, the Bayes-optimal denoiser is given by

⁹ QPSK is explicitly selected for simplicity, but wlg, denoisers for other modulation schemes can be also designed [86].

$$\hat{x}_{\bar{n},\bar{m}}^{(i)} = c_x \left(\tanh \left[2c_d \frac{\Re\{\bar{x}_{\bar{n},\bar{m}}^{(i)}\}}{\hat{\sigma}_{x:\bar{n},\bar{m}}^{2(i)}} \right] + j \tanh \left[2c_d \frac{\Im\{\bar{x}_{\bar{n},\bar{m}}^{(i)}\}}{\hat{\sigma}_{x:\bar{n},\bar{m}}^{2(i)}} \right] \right), \quad (66)$$

where $c_x \triangleq \sqrt{E_S/2}$ denotes the magnitude of the real and imaginary parts of the explicitly chosen QPSK symbols, with its corresponding variance updated as in (58).

After obtaining $\hat{x}_{\bar{n},\bar{m}}^{(i)}$ as per expression (66), the final outputs are computed by damping the results to prevent convergence to local minima due to incorrect hard-decision replicas [87]. Letting the damping factor be $0 < \beta_x < 1$, yields

$$\hat{x}_{\bar{n},\bar{m}}^{(i)} = \beta_x \hat{x}_{\bar{n},\bar{m}}^{(i)} + (1 - \beta_x) \hat{x}_{\bar{n},\bar{m}}^{(i-1)}, \quad (67)$$

Similarly, the variances $\hat{\sigma}_{x:\bar{n},\bar{m}}^{2(i)}$ are first updated via (58) and then damped via

$$\hat{\sigma}_{x:\bar{n},\bar{m}}^{2(i)} = \beta_x \hat{\sigma}_{x:\bar{n},\bar{m}}^{2(i)} + (1 - \beta_x) \hat{\sigma}_{x:\bar{n},\bar{m}}^{2(i-1)}, \quad (68)$$

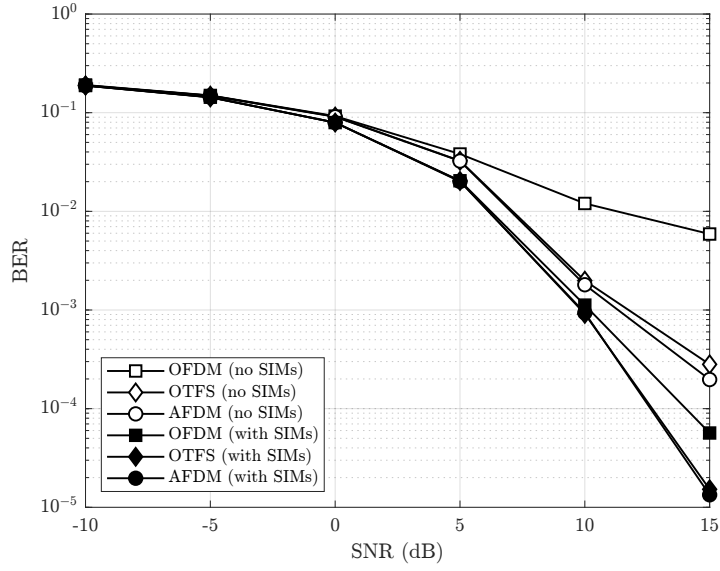
Finally, as result of the conflicting dimensions, the consensus update of the estimates can be obtained as follows:

$$\hat{x}_{\bar{m}} = \left(\sum_{\bar{n}=1}^{\bar{N}} \frac{|h_{\bar{n},\bar{m}}|^2}{\hat{\sigma}_{x:\bar{n},\bar{m}}^{2(i_{\max})}} \right)^{-1} \left(\sum_{\bar{n}=1}^{\bar{N}} \frac{h_{\bar{n},\bar{m}}^* \hat{y}_{x:\bar{n},\bar{m}}^{(i_{\max})}}{\hat{\sigma}_{x:\bar{n},\bar{m}}^{2(i_{\max})}} \right). \quad (69)$$

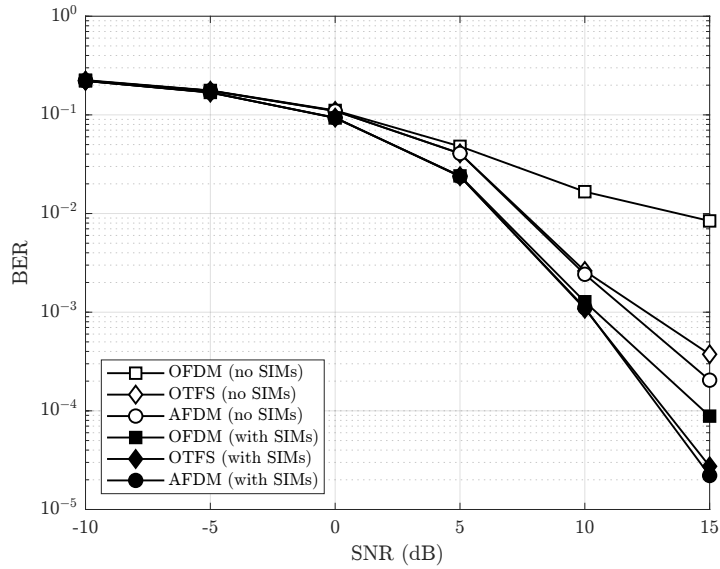
The complete pseudocode for the SIM parameterization and detection procedure here proposed is summarized in Algorithm 1.

5.3 Performance Analysis

In this section, simulation results for the bit error rate (BER) performances of OFDM, OTFS and AFDM systems with QPSK modulation in a SIM-enabled DD channel optimized via Algorithm 1 are provided. For the sake of simplicity, uplink single-input multiple-output (SIMO) and SISO scenarios are considered where both the TX and RX are equipped with SIM, and there are no RISs in the environment. All the other parameters are as in section 4.5, with the exception that the number of paths here is set to a more realistic $P = 5$ and the delay and Doppler shifts are randomly generated. In order to make sure that no power advantage other than the effect of the parametrized SIM is provided, the complete channels are normalized such that $\|\bar{\mathbf{H}}_{\text{OFDM}}\|_F^2 = \|\bar{\mathbf{H}}_{\text{OTFS}}\|_F^2 = \|\bar{\mathbf{H}}_{\text{AFDM}}\|_F^2 = \|\bar{\mathbf{H}}_{\text{MIMO}}\|_F^2$ for all the cases.



(a) SIMO: $N = 256$, $\tilde{K} = \tilde{K}' = 16$, $P = 5$, $N_T = 1$, $N_R = 4$, $d_s = 1$.



(b) SIMO: $N = 256$, $\tilde{K} = \tilde{K}' = 16$, $P = 5$, $N_T = 1$, $N_R = 2$, $d_s = 1$.

Fig. 3: BER Performance of OFDM, OTFS, and AFDM waveforms with QPSK modulation in MPDD channels with high-mobility, where SIM has been placed at very close distances to both the TX and the RX.

The results are shown in Fig. 3, from which it can be seen that the SIM-based systems significantly outperform those without SIM. It can be observed that other than the obvious reduction of BER resulting from the utilization of more receive antennas, the systems employing SIM exhibit very similar behaviors (see Fig. 4 for the SISO results), which indicates that the technology indeed has the potential to substantially lower the gap between more sophisticated (multi-antenna) and less sophisticated (single-antenna) systems. In fact, it can also be seen that having SIM significantly boosts the performance of conventional OFDM compared to its typical performance in a DD channel, bringing it close to that of far more sophisticated schemes, such as OTFS and AFDM.

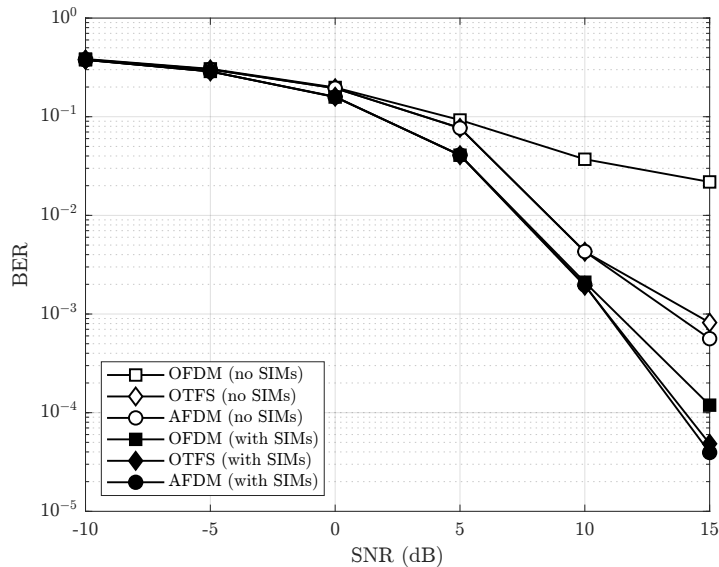


Fig. 4: Similar to Fig. 3 considering a SISO setting.

6 SIM Optimization and Radar Parameter Estimation

The focus of this section is RPE performance (i.e., sensing performance), and investigating the role of SIM for this functionality. To this end, the optimization problem presented in Section 5.1 is reformulated to align towards a more sensing-centric approach, and solved via a greedy gradient ascent, and complemented by a probabilistic data association (PDA)-based estimator following [25] to estimate the actual ranges and velocities of objects in the surrounding.

The system model considered is the same as Fig. 1, with the only difference being that the goal is to estimate radar parameters at the receiver in a bistatic fashion, with full knowledge of the transmit signal via pilots or a front-haul. Note that a blind

bistatic approach is also possible [32]. For simplicity, a SISO system equipped with SIM without RISs in the ambient is considered henceforth.

6.1 SIM-Based Signal Enhancement

Similarly to Section 5.1, the matrices \mathcal{Z} and $\tilde{\mathcal{Z}}$ must be parametrized to enhance the sensing performance by maximizing the power of the weakest path. To this end, define:

$$p_{\min} = \arg \min_p \left\| \mathbf{O}_p \right\|_F \quad (70)$$

selecting the path with the minimum power, $\mathbf{O}_{p_{\min}}$, which can be maximized egoistically:

$$\begin{aligned} \max_{\mathcal{Z}, \tilde{\mathcal{Z}}} O_{\min}(\mathcal{Z}, \tilde{\mathcal{Z}}) &= \left\| \mathbf{O}_{p_{\min}} \right\|_F^2 \\ \text{s.t. } \Upsilon_{\text{T}}(\mathcal{Z}) &\text{ as in eq. (11), } \Upsilon_{\text{R}}(\tilde{\mathcal{Z}}) \text{ as in eq. (12),} \\ \Psi_q &\text{ and } \Lambda_{\tilde{q}} \text{ as in eqs. (9) and (14), respectively,} \\ |\zeta_m^q| &\leq \pi \forall (q, m), \text{ and } |\tilde{\zeta}_{\tilde{m}}^{\tilde{q}}| \leq \pi \forall (\tilde{q}, \tilde{m}). \end{aligned} \quad (71)$$

In view of the non-convex unit modulus constraints, simple gradient-ascent technique is utilized in an iterative manner which tunes the phase shift parameters of the SIM in a greedy fashion. Following Section 5.1, the gradient expressions can be derived as:

$$\nabla_{\zeta_q} O_{\min}(\mathcal{Z}, \tilde{\mathcal{Z}}) = 2\Im \left\{ \sum_{n_t=1}^{N_T} \Psi_q^H \tilde{\Upsilon}_{t:q, p_{\min}, n_t}^H \mathbf{o}_{p_{\min}, n_t} \right\}, \quad (72)$$

and

$$\nabla_{\tilde{\zeta}_{\tilde{q}}} O_{\min}(\mathcal{Z}, \tilde{\mathcal{Z}}) = 2\Im \left\{ \sum_{n_t=1}^{N_T} \Lambda_{\tilde{q}}^H \tilde{\Upsilon}_{r:\tilde{q}, p_{\min}, n_t}^H \mathbf{o}_{p_{\min}, n_t} \right\}. \quad (73)$$

6.2 PDA-Based Estimation

Following [25], the PDA procedure can be concisely described as follows.

6.2.1 Problem Reformulation

Leveraging the fact that the DD channel can be characterized by a maximum normalized delay spread, $\max(\ell_p)$, and a corresponding digital normalized Doppler spread, $\max(f_p)$, satisfying the relations $\max(\ell_p) \ll N$ and $\max(f_p) \ll N$, for a finite

number P of paths, the channel impulse response in expression (3) can be rewritten as follows:

$$h^{\text{DD}}(\tau, \nu) = \sum_{\bar{k}=0}^{K_\tau-1} \sum_{\bar{d}=0}^{D_\nu-1} h_{\bar{k},\bar{d}} \delta(\tau - \tau_{\bar{k}}) \delta(\nu - \nu_{\bar{d}}), \quad (74)$$

where K_τ and D_ν are numbers large enough to define a sufficiently fine grid discretizing the region determined by the maximum delay and Doppler values. Notice that, if the resolution of such a grid is sufficiently fine, the only non-zero terms inside the summation in (74) are those where both $\tau_{\bar{k}} \approx \tau_p$ and $\nu_{\bar{d}} \approx \nu_p$, which in turn implies that estimating these radar parameters amounts to estimating the P channel gains such that $h_{\bar{k},\bar{d}} \neq 0$. This suggests that the RPE problem can be formulated as a canonical sparse signal recovery problem, as follows.

First, rewriting the time-continuous model of (74) in terms of the sampled equivalent in matrix form, yields the expression:

$$\tilde{\mathbf{H}}_{\text{RPE}} \triangleq \sum_{\bar{k}=0}^{K_\tau-1} \sum_{\bar{d}=0}^{D_\nu-1} \check{h}_{\bar{k},\bar{d}}^d \mathbf{G}_{\bar{k},\bar{d}}^{\text{RPE}}. \quad (75)$$

This model is identical to the equivalent channel implicitly defined in (42), only with the summation rewritten over the DD grid, as opposed to the channel paths, for a general waveform in a SISO system. Then, the generalized receive signal model given in (56) can be re-expressed as follows:

$$\mathbf{y} = \sum_{\bar{k}=0}^{K_\tau-1} \sum_{\bar{d}=0}^{D_\nu-1} \underbrace{\mathbf{G}_{\bar{k},\bar{d}}^{\text{RPE}} \mathbf{x}}_{\triangleq \mathbf{e}_{\bar{k},\bar{d}} \in \mathbb{C}^{N \times 1}} h_{\bar{k},\bar{d}} + \bar{\mathbf{w}} = \mathbf{E} \mathbf{h} + \bar{\mathbf{w}} \in \mathbb{C}^{N \times 1}, \quad (76a)$$

where the vectors are defined as $\mathbf{e}_{\bar{k},\bar{d}} \triangleq \mathbf{G}_{\bar{k},\bar{d}}^{\text{RPE}} \mathbf{x} \forall \bar{k}, \bar{d}$, and explicitly identified the dictionary matrix $\mathbf{E} \in \mathbb{C}^{N \times K_\tau D_\nu}$ and the sparse channel vector $\mathbf{h} \in \mathbb{C}^{K_\tau D_\nu \times 1}$:

$$\mathbf{E} \triangleq [\mathbf{e}_{0,0}, \dots, \mathbf{e}_{0,D_\nu-1}, \dots, \mathbf{e}_{K_\tau-1,0}, \dots, \mathbf{e}_{K_\tau-1,D_\nu-1}], \quad (76b)$$

$$\mathbf{h} \triangleq [h_{0,0}, \dots, h_{0,D_\nu-1}, \dots, h_{K_\tau-1,0}, \dots, h_{K_\tau-1,D_\nu-1}]^\top. \quad (76c)$$

In summary, the problem of estimating the set of radar parameters $\{\tau_p, \nu_p\} \forall p$ reduces to estimating the sparse channel vector \mathbf{h} , with the delays and Doppler shifts obtained from the corresponding indices (\bar{k}, \bar{d}) where $h_{\bar{k},\bar{d}} \neq 0$, given the received signal \mathbf{y} and the dictionary matrix \mathbf{E} . As a consequence of the approach, the assumption that P is known is relaxed into the assumption that the channel paths are orthogonal in the delay-Doppler grid, such that P can be unambiguously inferred from \mathbf{h} . Finally, the method also implies the assumption that the transmit vector \mathbf{x} is known at the radar receiver, which is in agreement with the considered bistatic setup.

6.2.2 PDA-Based Radar Parameter Estimation

In this section, a PDA-based RPE scheme designed under the assumption that the prior distributions of the elements $\hat{h}_{\check{m}}$ ¹⁰ of the sparse channel vector estimates $\hat{\mathbf{h}}$ are of Bernoulli-Gaussian type is presented. In other words, the unknown channel to be estimated at each i -th iteration of the proposed scheme is modelled as follows:

$$\hat{h}_{\check{m}}^{(i)} \sim p_{h_{\check{m}}}(\mathbf{h}_{\check{m}}; \boldsymbol{\theta}^{(i)}), \quad (77)$$

with

$$p_{h_{\check{m}}}(\mathbf{h}_{\check{m}}; \boldsymbol{\theta}^{(i)}) \triangleq (1-\rho^{(i)})\delta(h_{\check{m}}) + \rho^{(i)}\mathcal{CN}(h_{\check{m}}; \bar{h}^{(i)}, \bar{\sigma}^{(i)}), \quad (78)$$

where $\boldsymbol{\theta}^{(i)} \triangleq [\rho^{(i)}, \bar{h}^{(i)}, \bar{\sigma}^{(i)}]$ carries all three parameters of the distribution, namely, sparsity rate, mean, and variance. This parameter needs to be updated iteratively, and for this the EM algorithm is considered. For later convenience, the soft replica (i.e., tentative estimate) of $h_{\check{m}}$ as $\{\hat{h}_{\check{m}}^{(i)}\}$ can be defined, such that its MSE can be expressed as follows:

$$\hat{\sigma}_{h_{\check{m}}}^{2(i)} \triangleq \mathbb{E}_{h_{\check{m}}} [|h_{\check{m}} - \hat{h}_{\check{m}}^{(i)}|^2]. \quad (79)$$

Following steps similar to those in Section 5, the message passing algorithm is developed in the following manner.

Soft Interference Cancellation: The soft IC expression corresponding to an estimate of $h_{\check{m}}$, is given by

$$\tilde{\mathbf{y}}_{h_{\check{m}}}^{(i)} = \mathbf{y} - \sum_{q \neq \check{m}} \mathbf{e}_q \hat{h}_q^{(i)} = \mathbf{e}_{\check{m}} h_{\check{m}} + \overbrace{\sum_{q \neq \check{m}}^{K_{\tau} D_{\nu}} (\mathbf{e}_q h_q - \mathbf{e}_q \hat{h}_q^{(i)})}^{\text{residual interference+noise component}} + \tilde{\mathbf{w}}, \quad (80)$$

where $\mathbf{e}_{\check{m}}$ is the \check{m} -th column of the dictionary matrix \mathbf{E} . It follows from the central limit theorem (CLT) that, under large-system conditions, the residual interference-plus-noise component can be approximated by a multivariate complex Gaussian variate. In other words, the vector Gaussian approximation (VGA) can be applied such that the conditional PDF of the beliefs $\tilde{\mathbf{y}}_{h_{\check{m}}}^{(i)}$, given $h_{\check{m}}$, can be expressed as

$$\tilde{\mathbf{y}}_{h_{\check{m}}}^{(i)} \sim p_{\mathbf{y}|h_{\check{m}}}(\mathbf{y}|h_{\check{m}}) \propto \exp \left[-(\mathbf{y} - \mathbf{e}_{\check{m}} h_{\check{m}})^{\text{H}} \boldsymbol{\Sigma}_{\check{m}}^{-1(i)} (\mathbf{y} - \mathbf{e}_{\check{m}} h_{\check{m}}) \right], \quad (81)$$

where \mathbf{y} is an auxiliary variable, and the conditional covariance matrix $\boldsymbol{\Sigma}_{\check{m}}^{(i)}$, with σ_w^2 being the noise power, is given by

$$\begin{aligned} \boldsymbol{\Sigma}_{\check{m}}^{(i)} &\triangleq \mathbb{E}_{\mathbf{h}, \tilde{\mathbf{w}} | \hat{h}_{\check{m}} \neq h_{\check{m}}} \left[(\tilde{\mathbf{y}}_{h_{\check{m}}}^{(i)} - \mathbf{e}_{\check{m}} h_{\check{m}}) (\tilde{\mathbf{y}}_{h_{\check{m}}}^{(i)} - \mathbf{e}_{\check{m}} h_{\check{m}})^{\text{H}} \right] \\ &= \sum_{q \neq \check{m}}^{K_{\tau} D_{\nu}} \hat{\sigma}_{h_{\check{m}}}^{2(i)} \mathbf{e}_q \mathbf{e}_q^{\text{H}} + \sigma_w^2 \mathbf{I}_N. \end{aligned} \quad (82)$$

¹⁰ Wlgt, we set $\check{M} \triangleq K_{\tau} D_{\nu}$ for this section, with the corresponding elements $\check{m} = \{1, \dots, \check{M}\}$.

Belief Generation: The beliefs associated with the estimate of the \check{m} -th channel entry $h_{\check{m}}$ can be obtained by combining the contributions of all soft IC beliefs $\tilde{\mathbf{y}}_{h:\check{m}}^{(i)}$, under the PDF:

$$p_{h|h_{\check{m}}}(h|h_{\check{m}}) \propto \exp\left[-\frac{|h-\tilde{h}_{\check{m}}^{(i)}|^2}{\tilde{\sigma}_{h:\check{m}}^{2(i)}}\right], \quad (83)$$

which yields

$$\tilde{h}_{\check{m}}^{(i)} \triangleq \frac{1}{\eta_{\check{m}}^{(i)}} \mathbf{e}_{\check{m}}^H \Sigma^{-1(i)} \tilde{\mathbf{y}}_{h:\check{m}}^{(i)} \quad \text{and} \quad \tilde{\sigma}_{h:\check{m}}^{2(i)} \triangleq \frac{1 - \eta_{\check{m}}^{(i)} \hat{\sigma}_{h:\check{m}}^{2(i)}}{\eta_{\check{m}}^{(i)}}, \quad (84a)$$

where $\eta_{\check{m}}^{(i)}$ is a normalization factor defined as

$$\eta_{\check{m}}^{(i)} \triangleq \mathbf{e}_{\check{m}}^H \Sigma^{-1(i)} \mathbf{e}_{\check{m}}, \quad (84b)$$

and the common conditional covariance matrix¹¹ is given by

$$\Sigma^{(i)} \triangleq \sum_{\check{m}=1}^{K_{\tau} D_y} \hat{\sigma}_{h:\check{m}}^{2(i)} \mathbf{e}_{\check{m}} \mathbf{e}_{\check{m}}^H + \sigma_w^2 \mathbf{I}_N. \quad (84c)$$

Soft Replica Generation: Under VGA, as opposed to SGA for GaBP, the soft replicas of $h_{\check{m}}$ can be inferred from the conditional expectation given the extrinsic beliefs and the fact that the effective noise components in $\hat{h}_{\check{m}}^{(i)}$, $\forall \check{m}$ are uncorrelated, yielding:

$$p_{h_{\check{m}}|h}(h_{\check{m}}|h; \boldsymbol{\theta}^{(i)}) = \frac{p_{h|h_{\check{m}}}(h|h_{\check{m}}; \tilde{h}_{\check{m}}^{(i)}, \tilde{\sigma}_{h:\check{m}}^{2(i)}) p_{h_{\check{m}}}(h_{\check{m}}; \boldsymbol{\theta}^{(i)})}{\int_{h'_{\check{m}}} p_{h|h_{\check{m}}}(h|h'_{\check{m}}; \tilde{h}_{\check{m}}^{(i)}, \tilde{\sigma}_{h:\check{m}}^{2(i)}) p_{h_{\check{m}}}(h'_{\check{m}}; \boldsymbol{\theta}^{(i)})}. \quad (85)$$

Next, leveraging the assumption that $h_{\check{m}}$ follows a Bernoulli-Gaussian distribution and using the Gaussian-PDF multiplication rule [27], (85) can be rewritten as

$$p_{h_{\check{m}}|h}(h_{\check{m}}|h; \boldsymbol{\theta}^{(i)}) = (1 - \hat{\rho}_{\check{m}}^{(i)}) \delta(h_{\check{m}}) + \hat{\rho}_{\check{m}}^{(i)} \mathcal{CN}(h_{\check{m}}; \hat{h}_{\check{m}}^{(i)}, \hat{\sigma}_{h:\check{m}}^{2(i)}), \quad (86)$$

where

$$\hat{\rho}_{\check{m}}^{(i)} \triangleq \left(\frac{1 - \rho^{(i)}}{\rho^{(i)}} \frac{\tilde{\sigma}_{h:\check{m}}^{2(i)} + \bar{\sigma}^{(i)}}{\tilde{\sigma}_{h:\check{m}}^{2(i)}} e^{-\frac{|\tilde{h}_{\check{m}}^{(i)}|^2}{\tilde{\sigma}_{h:\check{m}}^{2(i)}} + \frac{|\tilde{h}_{\check{m}}^{(i)} - \bar{h}^{(i)}|^2}{\tilde{\sigma}_{h:\check{m}}^{2(i)} + \bar{\sigma}^{(i)}}} + 1 \right)^{-1} \quad (87)$$

with

$$\hat{h}_{\check{m}}^{(i)} \triangleq \frac{\bar{\sigma}^{(i)} \tilde{h}_{\check{m}}^{(i)} + \tilde{\sigma}_{h:\check{m}}^{2(i)} \bar{h}^{(i)}}{\tilde{\sigma}_{h:\check{m}}^{2(i)} + \bar{\sigma}^{(i)}} \quad \text{and} \quad \hat{\sigma}_{h:\check{m}}^{2(i)} \triangleq \frac{\bar{\sigma}^{(i)} \tilde{\sigma}_{h:\check{m}}^{2(i)}}{\tilde{\sigma}_{h:\check{m}}^{2(i)} + \bar{\sigma}^{(i)}}. \quad (88)$$

¹¹ The matrix inversion lemma is used in the derivation of (84) and by consequence (84b), such that the same inverse matrix $\Sigma^{(i)}$ can be used instead of $\Sigma_{\check{m}}^{(i)}$.

Finally, adhering to the prior defined for the channel coefficient h_p , wlg, a denoiser without the mean parameter, namely, $\bar{h}^{(i)} = 0$ in expression (78), and consequently, in (88) can be chosen¹². From (86), the soft replica $\hat{h}_{\check{m}}^{(i)}$ and its MSE $\hat{\sigma}_{h:\check{m}}^{2(i)}$ can be, in general, obtained from the conditional expectation as follows¹³:

$$\hat{h}_{\check{m}}^{(i)} = \tilde{\beta}_h \hat{\rho}_{\check{m}}^{(i)} \hat{h}_{\check{m}}^{(i)} + (1 - \tilde{\beta}_h) \hat{h}_{\check{m}}^{(i-1)}, \quad (89a)$$

$$\hat{\sigma}_{h:\check{m}}^{2(i)} = \tilde{\beta}_h [(1 - \hat{\rho}_{\check{m}}^{(i)}) \hat{\rho}_{\check{m}}^{(i)} |\hat{h}_{\check{m}}^{(i)}|^2 + \hat{\rho}_{\check{m}}^{(i)} \hat{\sigma}_{h:\check{m}}^{2(i)}] + (1 - \tilde{\beta}_h) [\hat{\sigma}_{h:\check{m}}^{2(i-1)}]. \quad (89b)$$

6.2.3 Parameter Update via EM

In order to update the parameter set θ of the Bernoulli-Gaussian distribution at each i -th iteration, the EM algorithm is utilized. In particular, EM is employed as an iterative parameter tuning technique to obtain the parameter vector θ that maximizes the likelihood function $p_{\mathbf{y}|\theta}(\mathbf{y}|\theta)$, where \mathbf{y} is defined in expression (76a) with θ given in (78). To this end, following [25], one can obtain the update rules as follows:

$$\rho^{(i)} = \frac{1}{K_\tau D_\nu} \sum_{\check{m}=1}^{K_\tau D_\nu} \hat{\rho}_{\check{m}}^{(i)}, \quad (90a)$$

$$\bar{h}^{(i)} = \frac{1}{K_\tau D_\nu \rho^{(i)}} \sum_{\check{m}=1}^{K_\tau D_\nu} \hat{\rho}_{\check{m}}^{(i)} \hat{h}_{\check{m}}^{(i)}, \quad (90b)$$

$$\bar{\sigma}^{(i)} = \frac{1}{K_\tau D_\nu \rho^{(i)}} \sum_{\check{m}=1}^{K_\tau D_\nu} \hat{\rho}_{\check{m}}^{(i)} \left(|\hat{h}_{\check{m}}^{(i)} - \bar{h}^{(i)}|^2 + \hat{\sigma}_{h:\check{m}}^{2(i)} \right). \quad (90c)$$

Remark 3 (Assumptions) Since the complex path gains $\tilde{h}_p, \forall p$ in equation (71) are generally unknown at the receiver for the SIM optimization prior to the estimation procedure, these can be set to unity in order to initialize the receiver with equal path powers. Additionally, the matrix $\mathbf{B}_p \forall p$ is assumed to be known via a prior estimation; in general, one can use a direction-of-arrival (DoA) estimation method as done in [24] to obtain a very accurate estimate of the AoAs and AoDs.

The complete pseudocode for the SIM parameterization and sensing procedure proposed is summarized in Algorithm 2.

¹² For completeness, the EM parameter update detailed in the consequent section will be derived for all the parameters.

¹³ Note the already incorporated damping procedure, as also done in Section 5, to prevent convergence to local minima due to incorrect hard-decision replicas.

Algorithm 2 SIM Optimization and RPE

Input: Receive signal vector \mathbf{y} , dictionary matrix \mathbf{E} , number of paths P , average channel power per path σ_h^2 , damping factor $\tilde{\beta}_h$, number of PDA iterations i_{\max} , number of gradient descent iterations i_{GD} , and noise variance σ_w^2 .

Output: Estimates $\hat{\tau}_p$ and \hat{v}_p extracted from the non-zero indices of the sparse channel estimate vector $\hat{\mathbf{h}}$.

Initialization

- Set counter to $i = 0$, and initial distribution parameters $\rho^{(0)} = P/(K_\tau D_\nu)$ and $\bar{\sigma}^{(0)} = 1/P$.
- Set average channel power per path as $\sigma_h^2 = 1/(K_\tau D_\nu)$.
- Set initial estimates $\hat{h}_{\tilde{m}}^{(0)} = 0$ and $\hat{\sigma}_{h:\tilde{m}}^{(0)} = \sigma_h^2 \forall \tilde{m}$.

SIM Optimization via Greedy Steepest Ascent

for $p = 1$ to $P + 1$

- 1: Compute p_{\min} using (70).
- for** $i = 1$ to i_{GD} **do** $\forall q, \tilde{q}, m, \tilde{m}$
- 2: Compute the gradients using expressions (49) and (53).
- 3: Update normalization parameters from (55).
- 4: Update the phase parameters via (54).

end for

end for

Radar Parameter Estimation via PDA

for $i = 1$ to i_{\max} **do** $\forall \tilde{m}$

- 5: Compute soft signal vectors $\tilde{\mathbf{y}}_{h:\tilde{m}}^{(i)}$ from equation (80).
- 6: Compute soft extrinsic channel beliefs $\tilde{h}_{\tilde{m}}^{(i)}$ and their variances $\tilde{\sigma}_{h:\tilde{m}}^{2(i)}$ from (84).
- 7: Compute denoised sparsity rates $\hat{\rho}_{\tilde{m}}^{(i)}$ from (87).
- 8: Compute denoised channel estimates $\hat{h}_{\tilde{m}}^{(i)}$ and their variances $\hat{\sigma}_{h:\tilde{m}}^{2(i)}$ via (88).
- 9: Compute damped channel estimates $\hat{h}_{\tilde{m}}^{(i)}$ and variances $\hat{\sigma}_{h:\tilde{m}}^{2(i)}$ using (89).
- 10: Update distribution parameters $\rho^{(i)}$ and $\bar{\sigma}^{(i)}$ from (90).

end for

- 11: Compute the estimates $\hat{\tau}_p$ and \hat{v}_p corresponding to the indices \tilde{m} of the non-zero entries of $\hat{\mathbf{h}}$ in accordance to expression (76c).

6.3 Sensing Performance Results

Fig. 5 illustrates the MSE performance of the aforementioned method with OFDM, OTFS, and AFDM signaling¹⁴ with QPSK modulation in a SIM-enabled DD channel, considering a SISO setting where both the TX and RX are equipped with SIM, and there are no RISs in the environment. It is assumed that the system operates with a carrier frequency of 28 GHz (*i.e.*, at wavelength $\lambda = 10.7$ mm) with a bandwidth of $B = 20$ MHz in an environment with identical TX and RX SIM, both with $Q = \tilde{Q} = 3$ layers of metasurfaces and $M = \tilde{M} = 100$ meta-atoms per layer, leading to $M_x = M_z = \tilde{M}_x = \tilde{M}_z = 10$. Finally, the sampling frequency is set to $F_S = B$ and

¹⁴ It was shown in [21, 25] that the communication-centric ISAC performance for OFDM, OTFS, and AFDM are very similar, which holds true even with the SIM.

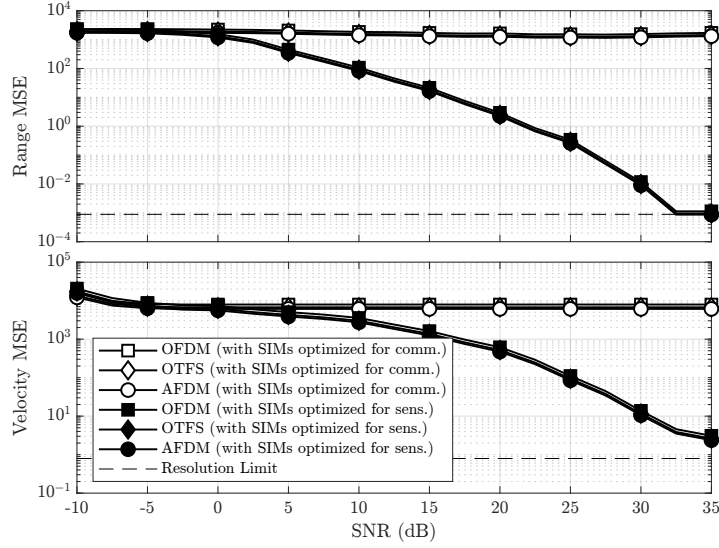


Fig. 5: MSE performance of OFDM, OTFS and AFDM waveforms with QPSK modulation in MPDD channels with high-mobility, with SIM placed at very close distances to both the TX and the RX in a SISO setting with $N = 144$, $\tilde{K} = \tilde{K}' = 12$, $P = 2$, $N_T = 1$, $N_R = 1$, $d_s = 1$.

the number of symbols per frame to $N = 144$. For the MPDD channel, the 2D and 3D elevation AoDs/AoAs are uniformly distributed in $[0, \pi]$, while the 3D azimuth AoDs/AoAs are in $[-\frac{\pi}{2}, \frac{\pi}{2}]$. Within the channel, there are two targets (*i.e.*, $P = 2$), with ranges 37.5 m and 97.5 m and velocities -54 m/s and $+54$ m/s, respectively.

In Fig. 5, the resolution limit defines how fine the search grid is, *i.e.*, it measures the estimation accuracy for the range and velocity if the estimate for $\hat{\mathbf{h}}$, obtained as the output of the proposed Algorithm 2, is perfect. As observed in the figure, there exists a large gain in performance when using the sensing-based optimization for the SIM, as opposed to the communication-based optimization presented in the previous Section 5.

6.4 ISAC Performance Results

A natural question that occurs is whether there is a fundamental tradeoff between the performance of the communication and sensing functionalities due to the worse performance of the SIM optimized for communications in a sensing setting. Under the same parameters as in the previous Section 6.3, the communications performance of the SIM optimized for sensing is also investigated. As seen from Fig. 6, while the communications performance decreases from the case where the SIM is optimized

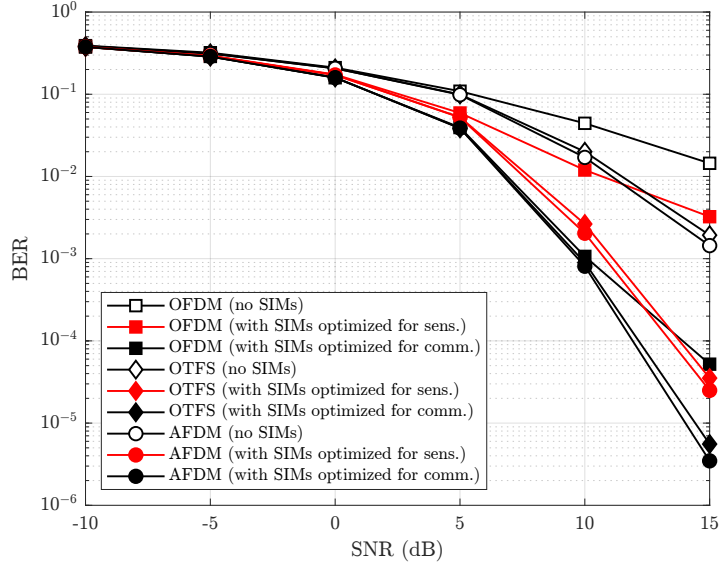


Fig. 6: BER performance of OFDM, OTFS and AFDM waveforms with QPSK modulation in MPDD channels with high-mobility, with SIM placed at very close distances to both the TX and the RX in a SISO setting with $N = 144$, $\tilde{K} = \tilde{K}' = 12$, $P = 2$, $N_T = 1$, $N_R = 1$, $d_s = 1$.

for communications, there is still a significant gain over the case where no SIM are used, highlighting the effectiveness of the SIM for ISAC, regardless of the waveform in use. However, it is noteworthy that the OFDM waveform exhibits a smaller performance enhancement as opposed to OTFS and AFDM when using the sensing optimized SIMs for communications, hinting at the usual superiority of OTFS and AFDM waveforms in DD channels [25].

7 Conclusions

In this chapter, the metasurfaces-parametrized DD MIMO channel model that integrates an arbitrary number of RISs in the environment, together with SIM at both the transmitter and receiver has been introduced, which is applicable to various ISAC-enabling waveforms. By explicitly formulating the I/O relationships for OFDM, OTFS, and AFDM, it was demonstrated how the proposed MPDD channel model could be effectively leveraged to optimize SIM, enhancing the performance of these waveforms in DD environments. The performance evaluation results indicated that SIM significantly improve system performance, helping to bridge the gap between advanced waveform designs, such as OTFS and AFDM, with the conventional OFDM.

References

1. S. Chen, J. Hu, Y. Shi, Y. Peng, J. Fang, R. Zhao, and L. Zhao, "Vehicle-to-Everything (V2X) Services Supported by LTE-Based Systems and 5G," *IEEE Commun. Stand. Mag.*, vol. 1, no. 2, 2017.
2. D. C. Nguyen, M. Ding, P. N. Pathirana, A. Seneviratne, J. Li, D. Niyato, O. Dobre, and H. V. Poor, "6G Internet of Things: A Comprehensive Survey," *IEEE Internet Things J.*, vol. 9, no. 1, 2022.
3. J. Shi, Z. Li, J. Hu, Z. Tie, S. Li, W. Liang, and Z. Ding, "OTFS Enabled LEO Satellite Communications: A Promising Solution to Severe Doppler Effects," *IEEE Network*, vol. 38, no. 1, 2024.
4. J. Li, Y. Niu, H. Wu, B. Ai, S. Chen, Z. Feng, Z. Zhong, and N. Wang, "Mobility Support for Millimeter Wave Communications: Opportunities and Challenges," *IEEE Commun. Surveys Tuts.*, vol. 24, no. 3, 2022.
5. T. Wang, J. Proakis, E. Masry, and J. Zeidler, "Performance Degradation of OFDM Systems due to Doppler Spreading," *IEEE Trans. Wireless Commun.*, vol. 5, no. 6, 2006.
6. K. Liu, T. Kadous, and A. Sayeed, "Orthogonal Time-Frequency Signaling over Doubly Dispersive Channels," *IEEE Trans. Inf. Theory*, vol. 50, no. 11, 2004.
7. D. W. Bliss and S. Govindasamy, *Dispersive and Doubly Dispersive Channels*, Cambridge University Press, 2013.
8. H. S. Rou, G. T. F. de Abreu, J. Choi, D. González G., M. Kountouris, Y. L. Guan, and O. Gonsa, "From Orthogonal Time-Frequency Space to Affine Frequency-Division Multiplexing: A Comparative Study of Next-Generation Waveforms for Integrated Sensing and Communications in Doubly Dispersive Channels," *IEEE Signal Process. Mag.*, vol. 41, no. 5, 2024.
9. G. D. Surabhi, R. M. Augustine, and A. Chockalingam, "On the Diversity of Uncoded OTFS Modulation in Doubly-Dispersive Channels," *IEEE Trans. Wireless Commun.*, vol. 18, no. 6, 2019.
10. R. Bomfin, M. Chafii, A. Nimr, and G. Fettweis, "A Robust Baseband Transceiver Design for Doubly-Dispersive Channels," *IEEE Trans. Wireless Commun.*, vol. 20, no. 8, 2021.
11. A. Pfadler, T. Szollmann, P. Jung, and S. Stańczak, "Estimation of Doubly-Dispersive Channels in Linearly Precoded Multicarrier Systems using Smoothness Regularization," *IEEE Trans. Wireless Commun.*, vol. 23, no. 2, 2024.
12. Y. Liang, P. Fan, Q. Wang, and X. He, "Two-Dimensional Delay-Doppler Pilots and Channel Estimation for Multi-Antenna OTFS in Doubly Dispersive Channels," *IEEE Trans. Wireless Commun.*, vol. 23, no. 7, 2024.
13. H. Haif, S. E. Zegrar, and H. Arslan, "Novel OCDM Transceiver Design for Doubly-Dispersive Channels," *IEEE Trans. Veh. Technol.*, vol. 73, no. 8, 2024.
14. H. Zhang, S. Chen, W. Meng, J. Yuan, and C. Li, "Multiuser Association and Localization over Doubly Dispersive Multipath Channels for Integrated Sensing and Communications," *IEEE J. Sel. Areas Commun.*, vol. 42, no. 10, 2024.
15. F. Liu, Y. Cui, C. Masouros, J. Xu, T. X. Han, Y. C. Eldar, and S. Buzzi, "Integrated Sensing and Communications: Toward Dual-Functional Wireless Networks for 6G and Beyond," *IEEE J. Sel. Areas Commun.*, vol. 40, no. 6, 2022.
16. S. P. Chepuri, N. Shlezinger, F. Liu, G. C. Alexandropoulos, S. Buzzi, and Y. C. Eldar, "Integrated Sensing and Communications with Reconfigurable Intelligent Surfaces: From Signal Modeling to Processing," *IEEE Signal Process. Mag.*, vol. 40, no. 6, Sep. 2023.
17. N. González-Prelcic, M. F. Keskin, O. Kaitiokallio, M. Valkama, D. Dardari, X. Shen, Y. Shen, M. Bayraktar, and H. Wymeersch, "The Integrated Sensing and Communication Revolution for 6G: Vision, Techniques, and Applications," *Proc. IEEE*, early access, 2024.
18. B. Smida, G. C. Alexandropoulos, T. Riihonen, and M. A. Islam, "In-Band Full-Duplex MIMO Systems for Simultaneous Communications and Sensing: Challenges, Methods, and Future Perspectives," *IEEE Signal Process. Mag.*, vol. 41, no. 5, Sep. 2024.

19. H. S. Rou, G. T. F. de Abreu, D. González G., and O. Gonsa, "Integrated Sensing and Communications for 3D Object Imaging via Bilinear Inference," *IEEE Trans. Wireless Commun.*, vol. 23, no. 8, 2024.
20. H. S. Rou, G. T. Freitas de Abreu, D. G. G and O. Gonsa, "Asymmetric Bilinear Inference for Joint Communications and Environment Sensing," *2022 56th Asilomar Conference on Signals, Systems, and Computers*, Pacific Grove, CA, USA, 2022, pp. 1111-1115.
21. L. Gaudio, M. Kobayashi, G. Caire, and G. Colavolpe, "On the Effectiveness of OTFS for Joint Radar Parameter Estimation and Communication," *IEEE Trans. Wireless Commun.*, vol. 19, no. 9, 2020.
22. S. K. Mohammed, R. Hadani, A. Chockalingam, and R. Calderbank, "OTFS—A Mathematical Foundation for Communication and Radar Sensing in the Delay-Doppler Domain," *IEEE Inf. Theory Mag.*, vol. 2, no. 2, 2022.
23. A. Gupta, M. Jafri, S. Srivastava, A. K. Jagannatham, and L. Hanzo, "An Affine Precoded Superimposed Pilot based mmWave MIMO-OFDM ISAC System," *IEEE Open J. Commun. Soc.*, vol. 5, 2024.
24. K. R. R. Ranasinghe, H. S. Rou, and G. T. F. de Abreu, "Fast and Efficient Sequential Radar Parameter Estimation in MIMO-OTFS Systems," in *Proc. IEEE International Conference on Acoustics, Speech and Signal Processing (ICASSP)*, Seoul, South Korea, 2024.
25. K. R. R. Ranasinghe, H. S. Rou, G. T. F. De Abreu, T. Takahashi, and K. Ito, "Joint Channel, Data and Radar Parameter Estimation for AFDM Systems in Doubly-Dispersive Channels," *IEEE Trans. Wireless Commun.*, early access, 2024.
26. A. Bemani, N. Ksairi, and M. Kountouris, "Integrated Sensing and Communications with Affine Frequency Division Multiplexing," *IEEE Wireless Commun. Lett.*, vol. 13, no. 5, May 2024, 2024.
27. J. T. Parker, P. Schniter, and V. Cevher, "Bilinear Generalized Approximate Message Passing—Part I: Derivation," *IEEE Trans. Signal Process.*, vol. 62, no. 22, 2014.
28. H. Iimori, T. Takahashi, K. Ishibashi, G. T. F. de Abreu, and W. Yu, "Grant-Free Access via Bilinear Inference for Cell-Free MIMO with Low-Coherence Pilots," *IEEE Trans. Wireless Commun.*, vol. 20, no. 11, 2021.
29. T. Takahashi, H. Iimori, K. Ando, K. Ishibashi, S. Ibi, and G. T. F. de Abreu, "Bayesian Receiver Design via Bilinear Inference for Cell-Free Massive MIMO with Low-Resolution ADCs," *IEEE Trans. Wireless Commun.*, vol. 22, no. 7, 2023.
30. X. Yang, K. Lei, S. Peng, and X. Cao, "Blind Detection for Primary User based on the Sample Covariance Matrix in Cognitive Radio," *IEEE Commun. Lett.*, vol. 15, no. 1, 2011.
31. J. Bao, J. Nie, C. Liu, B. Jiang, F. Zhu, and J. He, "Improved Blind Spectrum Sensing by Covariance Matrix Cholesky Decomposition and RBF-SVM Decision Classification at Low SNRs," *IEEE Access*, vol. 7, 2019.
32. K. R. R. Ranasinghe, K. Ando, H. S. Rou, G. T. F. de Abreu, and A. Bathelt, "Blind Bistatic Radar Parameter Estimation in Doubly-Dispersive Channels," to appear in *Proc. IEEE Wireless Communications and Networking Conference (WCNC)*, Milan, Italy, 2025.
33. Y. Ni, Z. Wang, P. Yuan, and Q. Huang, "An AFDM-based Integrated Sensing and Communications," in *Proc. International Symposium on Wireless Communication Systems*, Hangzhou, China, 2022.
34. A. Bemani, N. Ksairi, and M. Kountouris, "Affine Frequency Division Multiplexing for Next Generation Wireless Communications," *IEEE Trans. Wireless Commun.*, vol. 22, no. 11, 2023.
35. H. S. Rou, K. Yukiyoishi, T. Mikuriya, G. T. F. de Abreu, and N. Ishikawa, "AFDM Chirp-Permutation-Index Modulation with Quantum-Accelerated Codebook Design," to appear in *Proc. IEEE 57th Asilomar Conference on Signals, Systems, and Computers (Asilomar CSSC)*, Pacific Grove, CA, USA, 2024.
36. S. D. Liyanaarachchi, T. Riihonen, C. B. Barneto, and M. Valkama, "Joint MIMO Communications and Sensing with Hybrid Beamforming Architecture and OFDM Waveform Optimization," *IEEE Trans. Wireless Commun.*, vol. 23, no. 2, 2024.
37. L. Gaudio, G. Colavolpe, and G. Caire, "OTFS vs. OFDM in the Presence of Sparsity: A Fair Comparison," *IEEE Trans. Wireless Commun.*, vol. 21, no. 6, 2022.

38. S. Srivastava and P. Hobden, "5GHz Chirp Signal Generator for Broadband FMCW Radar Applications," in *Proc. IEEE International Symposium on Smart Electronic Systems (iSES)*, 2018.
39. X. Ouyang and J. Zhao, "Orthogonal Chirp Division Multiplexing," *IEEE Trans. Commun.*, vol. 64, no. 9, 2016.
40. J. Tong, J. Yuan, H. Lin, and J. Xi, "Orthogonal Delay-Doppler Division Multiplexing (ODDM) over General Physical Channels," *IEEE Trans. Commun.*, vol. 72, no. 12, 2024.
41. Z. Wang *et al.*, "A Tutorial on Extremely Large-Scale MIMO for 6G: Fundamentals, Signal Processing, and Applications," *IEEE Commun. Surveys Tuts.*, vol. 26, no. 3, 2024.
42. P. Gavrilidis and G. C. Alexandropoulos, "Near-Field Beam Tracking with Extremely Massive Dynamic Metasurface Antennas," *IEEE Trans. Wireless Commun.*, early access, 2025.
43. E. Calvanese Strinati, G. C. Alexandropoulos, N. Amani, M. Crozzoli, G. Madhusudan, S. Mekki, F. Rivet, V. Sciancalepore, P. Sehier, M. Stark, and H. Wymeersch, "Towards distributed and intelligent integrated sensing and communications for 6G networks," *IEEE Wireless Commun.*, vol. 32, no. 1, pp. 60–67, 2025.
44. M. Jian, G. C. Alexandropoulos, E. Basar, C. Huang, R. Liu, Y. Liu, and C. Yuen, "Reconfigurable Intelligent Surfaces for Wireless Communications: Overview of Hardware Designs, Channel Models, and Estimation Techniques," *Intell. Converged Netw.*, vol. 3, no. 1, 2022.
45. I. Papoutsidakis and G. C. Alexandropoulos, "On the rate-exponent region of integrated sensing and communications with variable-length coding," in *Proc. IEEE Wireless Commun. Netw. Conf.*, Milan, Italy, 2025.
46. M. A. Islam, G. C. Alexandropoulos, and B. Smida, "Integrated sensing and communication with millimeter wave full duplex hybrid beamforming," in *Proc. IEEE Int. Conf. Commun.*, Seoul, South Korea, 2022.
47. I. Gavras, M. A. Islam, B. Smida, and G. C. Alexandropoulos, "Full duplex holographic MIMO for near-field integrated sensing and communications," in *Proc. European Signal Process. Conf.*, Helsinki, Finland, 2023.
48. G. C. Alexandropoulos, "Position aided beam alignment for millimeter wave backhaul systems with large phased arrays," in *Proc. IEEE Workshop Comput. Adv. in Multi-Sensor Adaptive Process.*, Curaçao, Dutch Antilles, 2017.
49. E. Basar, G. C. Alexandropoulos, Y. Liu, Q. Wu, S. Jin, C. Yuen, O. A. Dobre, and R. Schober, "Reconfigurable Intelligent Surfaces for 6G: Emerging Hardware Architectures, Applications, and Open Challenges," *IEEE Veh. Technol. Mag.*, vol. 19, no. 3, 2024.
50. Y. Liu, X. Liu, X. Mu, T. Hou, J. Xu, M. Di Renzo, and N. Al-Dhahir, "Reconfigurable Intelligent Surfaces: Principles and Opportunities," *IEEE Commun. Surveys Tuts.*, vol. 23, no. 3, 2021.
51. C. Pfeiffer and A. Grbic, "Cascaded Metasurfaces for Complete Phase and Polarization Control," *Appl. Phys. Lett.*, vol. 102, no. 23, 2013.
52. Y. Zhou, I. I. Kravchenko, H. Wang, J. R. Nolen, G. Gu, and J. Valentine, "Multilayer Noninteracting Dielectric Metasurfaces for Multiwavelength Metaoptics," *Nano. Lett.*, vol. 18, no. 12, 2018.
53. Y. Hu, X. Luo, Y. Chen, Q. Liu, X. Li, Y. Wang, N. Liu, and H. Duan, "3D-Integrated Metasurfaces for Full-Colour Holography," *Light Sci. Appl.*, vol. 8, no. 1, 2019.
54. D. Bliss and S. Govindasamy, *Dispersive and Doubly-Dispersive Channels*. Cambridge University Press, 2013.
55. Z. Wei *et al.*, "Orthogonal time-frequency space modulation: A promising next-generation waveform," *IEEE Wireless Communications*, vol. 28, no. 4, pp. 136–144, 2021.
56. J. J. Healy, M. A. Kutay, H. M. Ozaktas, and J. T. Sheridan, *Linear Canonical Transforms: Theory and Applications*. Springer, 2015, vol. 198.
57. Y. Hong, T. Thaj, and E. Viterbo, *Delay-Doppler Communications: Principles and Applications*. Academic Press, 2022.
58. S. Srivastava, R. K. Singh, A. K. Jagannatham, A. Chockalingam, and L. Hanzo, "OTFS Transceiver Design and Sparse Doubly-Selective CSI Estimation in Analog and Hybrid Beamforming aided mmWave MIMO Systems," *IEEE Trans. Wireless Commun.*, vol. 21, no. 12, 2022.

59. J. An, C. Yuen, C. Xu, H. Li, D. W. K. Ng, M. Di Renzo, M. Debbah, and L. Hanzo, "Stacked Intelligent Metasurface-aided MIMO Transceiver Design," *IEEE Wireless Commun.*, vol. 31, no. 4, 2024.
60. J. An, C. Yuen, Y. L. Guan, M. Di Renzo, M. Debbah, H. V. Poor, and L. Hanzo, "Two-Dimensional Direction-of-Arrival Estimation using Stacked Intelligent Metasurfaces," *IEEE J. Sel. Areas Commun.*, vol. 42, no. 10, 2024.
61. J. An, C. Xu, D. W. K. Ng, G. C. Alexandropoulos, C. Huang, C. Yuen, and L. Hanzo, "Stacked Intelligent Metasurfaces for Efficient Holographic MIMO Communications in 6G," *IEEE J. Sel. Areas Commun.*, vol. 41, no. 8, 2023.
62. M. Nerini, S. Shen, H. Li, and B. Clerckx, "Beyond Diagonal Reconfigurable Intelligent Surfaces utilizing Graph Theory: Modeling, Architecture Design, and Optimization," *IEEE Trans. Wireless Commun.*, vol. 23, no. 8, 2024.
63. D. Wijekoon, A. Mezghani, G. C. Alexandropoulos, and E. Hossain, "Physically-Consistent Modeling and Optimization of non-local RIS-Assisted Multi-User MIMO Communication Systems," *arXiv preprint:2406.05617*, 2024.
64. Z. R. Omam, H. Taghvaei, A. Araghi, M. García-Fernandez, G. Álvarez-Narciandi, G. C. Alexandropoulos, O. Yurduseven, and M. Khalily, "Holographic metasurfaces enabling wave computing for 6G: Status overview, challenges, and future research trends," *arXiv preprint:2501.05173*, 2025.
65. K. R. R. Ranasinghe, H. S. Rou, I. A. M. Sandoval, G. T. F. de Abreu, "A doubly-dispersive MIMO channel model with stacked intelligent metasurfaces," *arXiv preprint:2501.07724*, 2025.
66. K. Stylianopoulos, P. Di Lorenzo, and G. C. Alexandropoulos, "Over-the-air edge inference via end-to-end metasurfaces-integrated artificial neural networks," *arXiv preprint:2504.00233*, 2025.
67. G. C. Alexandropoulos and I. Gavras, "Extremely large full duplex MIMO for simultaneous downlink communications and monostatic sensing at sub-THz frequencies," *arXiv preprint:2502.10693*, 2025.
68. M. Matthaiou, G. C. Alexandropoulos, H. Q. Ngo, and E. G. Larsson, "Analytic framework for the effective rate of MISO fading channels," *IEEE Trans. Commun.*, vol. 60, no. 6, pp. 1741–1751, 2012.
69. G. C. Alexandropoulos, N. C. Sagias, F. I. Lazarakis, and K. Berberidis, "New results for the multivariate Nakagami-m fading model with arbitrary correlation matrix and applications," *IEEE Trans. Wireless Commun.*, vol. 8, no. 1, pp. 245–255, 2009.
70. K. P. Peppas, G. C. Alexandropoulos, C. K. Datsikas, and F. I. Lazarakis, "Multivariate Gamma-Gamma distribution with exponential correlation and its applications in RF and optical wireless communications," *IET Microwaves, Ant. & Prop.*, vol. 5, no. 3, pp. 364–371, 2011.
71. G. C. Alexandropoulos, D.-T. Phan-Huy, K. D. Katsanos, M. Crozzoli, H. Wymeersch, P. Popovski, P. Ratajczak, Y. Bénédic, M.-H. Hamon, S. Herraiz Gonzalez, P. Mursia, M. Rossanese, V. Sciancalepore, J.-B. Gros, S. Terranova, G. Gradoni, P. Di Lorenzo, M. Rahal, B. Denis, R. D'Errico, A. Clemente, and E. Calvanese Strinati, "RIS-enabled smart wireless environments: Deployment scenarios, network architecture, bandwidth and area of influence," *EURASIP J. Wireless Commun. Netw.*, 103, pp. 1–38, 2023.
72. K. R. R. Ranasinghe, Y. Ge, G. T. F. de Abreu, and Y. L. Guan, "Joint Channel Estimation and Data Detection for AFDM Receivers With Oversampling," to appear in *Proc. International Conference on Computing, Networking and Communications (ICNC)*, Honolulu, HI, USA, 2025.
73. R. Hadani, S. Rakib, M. Tsatsanis, A. Monk, A. J. Goldsmith, A. F. Molisch, and R. Calderbank, "Orthogonal Time Frequency Space Modulation," in *Proc. IEEE Wireless Communications and Networking Conference (WCNC)*, San Francisco, USA, 2017.
74. P. Raviteja, K. T. Phan, Y. Hong, and E. Viterbo, "Interference Cancellation and Iterative Detection for Orthogonal Time Frequency Space Modulation," *IEEE Trans. Wireless Commun.*, vol. 17, no. 10, 2018.

75. J. Zhu, Y. Tang, X. Wei, H. Yin, J. Du, Z. Wang, and Y. Liu, "A Low-Complexity Radar System based on Affine Frequency Division Multiplexing Modulation," *arXiv preprint arXiv:2312.11125*, 2023.
76. G. Liu, T. Mao, R. Liu, and Z. Xiao, "Pre-Chirp-Domain Index Modulation for Affine Frequency Division Multiplexing," *arXiv preprint arXiv:2402.15185*, 2024.
77. D. Tse, P. Viswanath, and L. Zheng, "Diversity-Multiplexing Tradeoff in Multiple-Access Channels," *IEEE Trans. Inf. Theory*, vol. 50, no. 9, 2004.
78. A. F. Molisch, V. V. Ratnam, S. Han, Z. Li, S. L. H. Nguyen, L. Li, and K. Haneda, "Hybrid Beamforming for Massive MIMO: A Survey," *IEEE Commun. Mag.*, vol. 55, no. 9, 2017.
79. K. D. Katsanos, P. Di Lorenzo, and G. C. Alexandropoulos, "Multi-RIS-empowered multiple access: A distributed sum-rate maximization approach," *IEEE J. Sel. Topics Signal Process.*, vol. 18, no. 7, pp. 1324–1338, 2024.
80. C. Huang, A. Zappone, G. C. Alexandropoulos, M. Debbah, and C. Yuen, "Reconfigurable intelligent surfaces for energy efficiency in wireless communication," *IEEE Trans. Wireless Commun.*, vol. 18, no. 8, pp. 4157–4170, 2019.
81. N. Shlezinger, G. C. Alexandropoulos, M. F. Imani, Y. C. Eldar, and D. R. Smith, "Dynamic metasurface antennas for 6G extreme massive MIMO communications," *IEEE Wireless Commun.*, vol. 28, no. 2, pp. 106–113, 2021.
82. L. You, J. Xu, G. C. Alexandropoulos, J. Wang, W. Wang, and X. Gao, "Energy efficiency maximization of massive MIMO communications with dynamic metasurface antennas," *IEEE Trans. Wireless Commun.*, vol. 22, no. 1, pp. 393–407, 2023.
83. L. Wei, C. Huang, G. C. Alexandropoulos, Z. Yang, J. Yang, W. E. I. Sha, Z. Zhang, M. Debbah, and C. Yuen, "Tri-polarized holographic MIMO surface in near-field: Channel modeling and precoding design," *IEEE Trans. Wireless Commun.*, vol. 22, no. 12, pp. 8828–8842, 2023.
84. I. A. M. Sandoval, K. Ando, O. Taghizadeh, and G. T. F. De Abreu, "Sum-Rate Maximization and Leakage Minimization for Multi-User Cell-Free Massive MIMO Systems," *IEEE Access*, vol. 11, 2023.
85. J. An, C. Yuen, Y. L. Guan, M. Di Renzo, M. Debbah, H. V. Poor, and L. Hanzo, "Stacked Intelligent Metasurface performs a 2D DFT in the Wave Domain for DOA Estimation," in *Proc. IEEE International Conference on Communications (ICC)*, Denver, CO, USA, 2024.
86. T. Takahashi, S. Ibi, and S. Sampei, "Design of Adaptively Scaled Belief in Multi-Dimensional Signal Detection for Higher-Order Modulation," *IEEE Trans. Commun.*, vol. 67, no. 3, 2019.
87. Q. Su and Y.-C. Wu, "On Convergence Conditions of Gaussian Belief Propagation," *IEEE Trans. Signal Process.*, vol. 63, no. 5, 2015.